EFFECT OF INTERNAL LOAD AND TEMPERATURE ON GRADED SPHERICAL SHELL

Dissertation submitted in partial fulfilment of the requirements

for the award of degree

of

Master of Technology in Marine Engineering and Management

by

SANJAY BALMIKI

(Reg.No.2101215005)

Under the Guidance of

Dr. SUJOY SAHA

Department of Marine Engineering

INDIAN MARITIME UNVERSITY

(A Central University, Government of India)

Indian Maritime University, Kolkata Campus

Kolkata - 700088

July 2023

Department of Marine Engineering
INDIAN MARITIME UNVERSITY
(A Central University, Government of India)
KOLKATA -700088, INDIA

CERTIFICATE

This is to certify that the thesis entitled **"EFFECT OF INTERNAL LOAD AND TEMPERATURE ON GRADED SPHERICAL SHELL"** submitted by **Mr. SANJAY BALMIKI (2101215005)** of the Department of Marine Engineering, Indian Maritime University (Kolkata Campus), in partial fulfilment of the requirements for the award of the degree of **Master of Technology** in Marine Engineering and Management, is a record of bonafide research work carried out under my supervision and guidance.

The content of the thesis does not form a basis for the award of other degrees to his/her, to the best of my knowledge. The thesis, in my opinion, is worthy of consideration for the award of the degree of **Master of Technology** in Marine Engineering and Management in accordance with the regulation of the Institute.

Dr. Sujoy Saha
Supervisor
Department of Marine Engineering
Indian Maritime University, Kolkata campus
Kolkata – 700888, India

Dr. Deepak Mishra
Course coordinator (MTech)
MTech Marine Engineering and Management
Indian Maritime University, Kolkata campus
Kolkata – 700888, India

COPYRIGHT AND CONSENT FORM

To ensure uniformity of treatment among all contributors, other forms may not be substituted for this form, nor may any wording of the form be changed. This form is intended for original material submitted to the Indian Maritime University, Kolkata Campus (IMU-KC), Kolkata and must accompany any such material in order to be published by the (IMU-KC). Please read the form carefully and keep a copy for your files.

TITLE OF THESIS: EFFECT OF INTERNAL LOAD AND TEMPERATURE ON GRADED SPHERICAL SHELL.

AUTHOR'S NAME and ADDRESS: SANJAY BALMIKI, A-701, Vrindavan Palms, Wayale Nagar, Kalyan West, 421301, Mumbai, Maharashtra.

COPY RIGHT TRANSFER

1. The undersigned hereby assigns to Indian Maritime University, Kolkata Campus (IMU-KC), Kolkata, all rights under copyright that may exist in and to: (a) the above work, including any revised or expanded derivative works submitted to the (IMU-KC), by the undersigned based on the work and (b) any associated written or multimedia components or other enhancements accompanying the work.

CONSENT AND RELEASE

2. In the event the undersigned makes a presentation based upon the work at a conference hosted or sponsored in whole or in part by the (IMU-KC), the undersigned, in consideration for his/her participation in the conference, hereby grants the (IMU-KC), the unlimited, worldwide, irrevocable permission to use, distribute, publish, license, exhibit, record, digitize, broadcast, reproduce and archive; in any format or medium, Whether now known or hereafter developed: (a) his /her presentation and comments at the conference; (b) any written materials or multimedia files used in connection with his/her presentation and; (c) any recorded interview him/her (collectively, the “Presentation"). The permission granted includes the transcription and reproduction of the Presentation for inclusion in products sold or distributed by (IMU-KC) and live or recorded broadcast of the Presentation during or after the conference.

3. In connection with the permission granted in Section 2, the undersigned hereby grants (IMU-KC) the unlimited, worldwide, irrevocable right to use his/her name, picture, likeness, voice and biographical information as part of the advertisement, distribution and sale of products incorporating the Work or Presentation, and releases (IMU-KC) from any claim based on right of privacy or publicity.

4. The undersigned hereby warrants that the Work and Presentation (collectively, the "Materials") are original and that he/she is the author of the Materials. To the extent the Materials incorporate test passages, figures, data or other material from the works of others, the undersigned has obtained any necessary permissions

GENERAL TERMS

- The undersigned represents that he/she has the power and authority to make and execute this assignment.
- The undersigned agrees to indemnify and hold harmless the (IMU-KC) from any damage or expense that may arise in the event of a breach of any of the warranties set forth above.
- In the event the above work is not accepted and published by the (IMU-KC) or is withdrawn by the author(s) before acceptance be the (IMU-KC), the foregoing copyright transfer shall become null and void and all materials embodying the work submitted to the (IMU-KC) will be destroyed.
- For jointly authored works, all joint authors should sign, or one of the authors should sign as authorized agent for the others.

Signature of the Author

DECLARATION

I certify that

(a) The work contained in this thesis is original and has been done by me under the guidance of my supervisors.

(b) The work has not been submitted to any other Institute for any degree or diploma.

(c) I have followed the guidelines provided by the Institute in preparing the thesis.

(d) I have conformed to the norms and guidelines given in the Ethical Code of Conduct of the Institute.

(e) Whenever I have used materials (data, theoretical analysis, figures, and text) from other sources, I have given due credit to them by citing them in the text of the thesis and giving their details in the references.

SANJAY BALMIKI

CONTENTS

ACKNOWLEDGEMENTS

It is my proud privilege to acknowledge the help and guidance received in preparation and presentation of this report. It would not have been possible to prepare this report in this form without valuable help, co-operation and constant guidance. First and foremost, I wish to record my sincere gratitude to Department of Marine Engineering, IMU Kolkata and to our beloved Director R Adm. (Retd.) Rangachari P J of Indian Maritime University for this constant support and encouragement in preparation of this report and making available library and laboratory facilities needed to prepare this report.

My sincere thanks to Professor and guide Dr. Sujoy Saha, Department of Marine Engineering, IMU Kolkata, for his valuable suggestions, reviews and sharing his valuable time by guiding me on investigations and presentation for this research work throughout the period of this report.

I express my sincere gratitude to the course coordinator, Dr. Deepak Mishra Department of Marine Engineering, IMU Kolkata, for his motivation and support in completion of the project report.

LIST OF FIGURES

LIST OF TABLES

ABSTRACT

In this work, the effect of internal pressure in a functionally graded hollow spherical shell is theoretically studied. The material properties through the graded direction are assumed to be non-linear with power law distribution. In order to obtain the effect of internal pressure and temperature on the design of pressure vessel, Navier and heat conduction equations are solved by direct method. The pressure variation and the mechanical stress distribution such as radial stress distribution and hoop stress distribution along the radial direction are presented in a sequential manner. The radial distribution of temperature has also been depicted in the result and discussion section. As a result of which it may be concluded that the material which has lower power law index is beneficial in terms of generation of lower thermal stress. The study also aims to understand the influence of autofrettage on stress distribution and load bearing capacity in thick spherical shells. Analytical equations, based on the Maximum Shear Stress theory and Distortion Energy theory, are derived to determine the optimum radius of the elastic-plastic juncture, known as C_{opt} in autofrettage technology. The results demonstrate that autofrettage increases the pressure inside the shell, enhancing its ability to withstand higher internal pressures.

CHAPTER 1

INTRODUCTION

Pressure vessels are essential components in various engineering applications, including aerospace, chemical, and oil and gas industries. Understanding the behavior of pressure vessels under internal pressure and temperature is crucial for their safe and efficient design. Autofrettage technology has been introduced in the early 1900s in order to reduce the number of accidents due to bursts of pressure vessels. In this technology, high internal pressure has been given to the pressure vessel and suddenly released as a result of which residual stress is generated following the elasto-plastic theory. The generation of radial stress is directly proportional to the radius of the spherical vessel, so the inner layer is subjected to more stress which is beyond the yield stress, consequently, plastic deformation is been taken place in this layer. On the other hand, the outer zone of the spherical shell is subjected to less stress, which is well below the yield stress, as a result of which elastic deformation has occurred at the outer zone. After releasing the pressure, the inner plastic zone is not able to regain its original shape but the outer elastic zone tried to regain its initial shape which is not possible due to the presence of the inner plastic zone. Therefore, inward residual stress is generated and acts on the inner layer. That residual stress counterbalances the applied internal pressure consequently, so the pressure vessel can withstand more internal pressure without failure. The inward residual stresses significantly improve the load-bearing capacity, fatigue resistance, and overall strength of the spherical shell, thereby enhancing its performance under operating conditions. In order to understand the effect of internal load and temperature on pressure vessels, different researchers have performed theoretical and experimental investigations. Among them, Anthony P. Parker et al. (2007) have considered the extended numerical procedure to solve the analogous problem of a spherical thick-walled steel vessel. A new equivalent analytical solution for the case of a spherical vessel has been formulated by them. It has been demonstrated numerically by them that a reautofrettage procedure, previously proposed for cylindrical vessels, could be extremely beneficial for spherical vessels. The procedure has been considered by them, and the tube to be autofrettaged has been divided into several thin tubular strips for numerical analysis, where each strip is in the form of a thin tube and is obliged to satisfy the requirement of equilibrium and compatibility at its inner and outer interfaces where it interacts with adjacent tubes. In this work, the potential benefit from reautofrettage of autofrettage tubes has been indicated, and their further purpose is to examine options for the reautofrettage of a spherical vessel. It has been found by them that the analytic solution is

nonconservative, and the analytic bore hoop stress is approximately 9% more compressive than the numerical solution for a compressive material with a varying unloading profile.

M. Jabbari et al. (2002) have presented a direct method to solve the Navier equation. They have considered a thick hollow cylinder of FGM under a one-dimensional steady-state temperature distribution with general types of thermal and mechanical boundary conditions. They have derived navier equation in terms of displacement and solved analytically by the direct method. They have also presented an analytical solution for the calculation of the axisymmetric thermal and mechanical stresses in a thick hollow cylinder made of FGM. They have assumed material properties through the graded direction to be nonlinear with a power law distribution.

Jesús Manuel Alegre Calderon et al. (2005) have considered a design of High-pressure vessel which can withstand huge cyclic loading and unloading under high pressure. In this article, a thick-walled vessel with autofrettage operating at an internal pressure of 500 Mpa, an internal diameter of 300 mm, and a length of 4500mm has been designed by them. Finite element analysis has been performed by them to determine the residual stresses after autofrettage at an internal pressure of 925 Mpa. The material of the vessel has been selected by them, which is made of stainless steel 15-5 PH (15Cr – 5Ni) and is hardened by precipitation and has a strong Bauschinger effect. In order to perform HPP (High pressure processing), the material at high pressure has been considered in a large container, which is capable of pasteurizing large quantities of the product. Water has been considered as a medium that will transmit the pressure, up to p_w =500 MPa in the present container, and it also helps to achieve the life of the high-pressure machine to make it economical. More than 100000 working cycles have been used by them. It has been observed by them that the material model with a loading curve is different from the unloading curve. Due to the consideration of the Bauschinger effect, a 25% reduction in residual stresses has been seen. It has been found by them that when the autofrettage pressure value is exceeded, residual stresses increase only slightly, whereas the plastic strains achieved during the autofrettage loading have been increased exponentially.

W.S. Shim et al. (2010) have introduced compressive residual stresses in the autofrettage process, which acts to offset the tensile residual stress induced by internal pressure. It has been noted by them that as the autofrettage level increases, the magnitude of compressive residual stresses at the bore also increases. The accurate residual stress of SNCM 8 high-strength steel has been predicted by them using the Kendall model, which is adopted by the ASME code, and the result has been compared with analytical and finite element analysis. It has been found by them that the residual stress incorporating the Bauschinger effect at the bore was smaller than

the ideal calculation. Tensile tests have been performed by them on the mechanical properties of SNCM 8 high-strength steel, where they obtained elastic modulus, yield strength, ultimate strength, elongation, and reduction of area. It has been noticed by them that as the autofrettage level increases, a greater autofrettage pressure is needed. Also, as the autofrettage level increases, the induced tangential residual stress at the bore and plastic strain increase. They have concluded that as the autofrettage level increases, the magnitude of induced tangential residual stress at the bore also increases, and the results of analytical and FE analysis are almost similar.

Rahman Seifi et al. (2011) have observed that the bursting pressure decreases considerably to 30% due to external cracks in the cylinders without autofrettage. The numerical and experimental results have been compared, showing that the bursting pressure of the autofrettaged cracked cylinder can be acceptably predicted by numerical methods. The distributions of residual stresses in thick-walled cylinders due to autofrettage cylinders have also been shown. They have seen that the Bauschinger effect changes the distribution of residual stress within one quarter of the wall thickness. The optimized autofrettage pressure for the largest bursting pressure has been achieved when the cross-section becomes fully plastic (100% autofrettage), but the number of autofrettage stages has no effect on the pressure capacity. The effect of the re-autofrettage procedure has been investigated by numerical method. The 'contact' option of the finite element software (Abaqus) has been used for simulating the autofrettage process in the cracked cylinder. It has been concluded that the bursting pressure of cracked components can be predicted using fracture toughness.

Sujoy Saha et al. (2011) have investigated the influence of autofrettage on stress distribution and load bearing capacity of a thick spherical shell. It has been observed that to achieve a suitable initial stress pattern inside the wall of a spherical shell, autofrettage is an appropriate method to obtain the optimum radius of elastic-plastic juncture, C_{opt}, where the equivalent stress σ_{eq} is minimum. In this work, the objective was to find an accurate analytical equation to determine C_{opt}. It has been concluded by the researchers that tension in the inner wall of the spherical shell is significantly reduced by autofrettage, and a favorable stress pattern can be obtained. It has also been found that an autofrettage treated spherical shell has limitless strength if the thickness is increased infinitely.

Zhong Hu et al. (2012) have numerically investigated the internal pressure overloading autofrettage process of a thick-walled cylinder. The optimum autofrettage pressure and the maximum reduction percentage of the von Mises stress in the autofrettaged cylinder under the

elastic-limit working pressure have been found by them. The differences in stress and strain distribution between adopting the Bauschinger-effect and the Non-Bauschinger effect have been compared by them. Autofrettage treatment has been used on the cylinder by Daniels (1942) and Masu and Graggs (1992) to prevent failure and to increase the pressure carrying capacity. The element PLANE183 with the capacity of elastic and plastic material nonlinearity and non-linear kinematic hardening (the Bauschinger effect), which is an eight-node plane-stress 2-D element with higher accuracy quadratic shape function has been adopted by them. In this work, more elements have been used near the inner surface and outer surface of the cylinder to get reasonable accuracy. Lame's equations have been used by them for calculating the hoop stress (σ_θ) and radial stress (σ_r) along the thickness of the cylinder when the ends of the cylinder are open and unconstrained so that the cylinder is in a condition of plane stress. The geometric and material condition has been considered by them, and the optimum autofrettage pressure has been found to be about 1.5 times the elastic-limit working pressure. The maximum reduction percentage of the maximum von Mises stress in the autofrettaged thick-walled cylinder under the elastic-limit working pressure has been found to be about 28%.

Niranjan Kumar (2012) have designed a pressure vessel to withstand high internal pressure for the same consumption of material. They have constructed a multilayer pressure vessel by shrink-fitting the vessel, which has residual stress within it caused by pre-autofrettage, followed by autofrettage of the assembly. Possible ways to assemble a three-layered vessel for different autofrettage or reautofrettage percentages and radial interference for shrink-fit have been discussed by them. Residual stresses generated at the inner and outer surface of the vessel due to autofrettaging or shrink-fitting have been observed to be of compressive and tensile nature, respectively. While optimizing the fatigue life, it has been observed that sometimes the net resulting hoop stress at the outer or middle layer is subjected to extreme tensile stress, which exceeds the design limit. It has been assumed by them that the strain produced on the outer surface of the combination is regained to its original dimensions by a surface finishing operation. The net effect of autofrettage and re-autofrettage has been calculated by the summation of the residual stress distribution along thickness, generated by autofrettage and reautofrettage. In this work, stress generated due to autofrettage and reautofrettage has been much below the yield point. Genetic algorithm, which is a class of probabilistic optimization algorithm based on the steps of natural genetics, has been introduced by them. A genetic algorithm has been used by them to maximize the fatigue life for a specific set of assembly parameters, which have been obtained as the optimum value of design variables in GA.

Pankaj Thakur (2012) have discussed the problem of elastic-plastic and creep of spherical shells under internal pressure. Simplifying assumptions have been applied by them, due to which problems like infinitesimal deformation and incompressibility of the material have been analyzed. Analysis of stresses in a spherical shell subjected to internal pressure has been performed by using Seth's transition theory by taking lebesgue measures. The result has been discussed numerically and depicted graphically by them. It has been mentioned by them that the spherical shell considered is subjected to a uniform temperature. It has been observed by them that a spherical shell made of compressible materials, such as copper and brass, and with a smaller radii ratio, yields at the internal surface, requiring a lesser value of pressure. It has been noted by them that circumferential stress is maximum at the external surface for compressible materials. Therefore, with increased compressibility, circumferential stresses decrease much.

M. Sedighi et al. (2013) have analyzed the effects of wire-winding on an autofrettaged thick-walled vessel. Results for the wire-wound autofrettage vessel have been obtained by them, by validating the finite element method. It has been seen by them that the residual hoop stresses in a wire-wound autofrettaged vessel have a more desirable distribution in the cylinder. In the autofrettage process, the internal surface of a thick-walled vessel is pressurized so that the inner part of its wall deforms plastically, and when the internal pressure is released, residual compressive stresses at the inner part of the cylinder are obtained. It has been seen by them that residual stress will increase the internal pressure capacity and improve the fatigue lifetime. It has been noted by them that autofrettage is a more convenient process but produces tensile stress in the outer part of the cylinder wall. Also, it has been seen by them that the maximum available compressive hoop stress is limited in the process, while in the wire-winding technique, there is no residual stress limitation. It has been observed by them that wire-winding is a safe technique that prevents rapid failure and introduces compressive residual stress in the whole cylinder wall. It has been concluded by them that the combination of these two techniques could have better benefits in comparison to the solo application of them. The direct method has been performed by them where results of residual hoop stress for the wire-wound autofrettaged vessel have been compared to residual hoop stresses before the wire-winding process. It has been noted by them that by increasing the number of wire layers or winding stress, it is possible to obtain a wire-wound autofrettaged vessel with only compressive hoop stress in the whole cylinder.

D. Dinesh Babu et al. (2013) have applied numerical simulation for the autofrettage process to a cylinder of known dimensions with the objective to provide a better understanding of the stresses that are developed at high pressure. Reduction in stress levels between autofrettaged and non-autofrettaged cylinders has been compared by them. It has been observed by them that at an autofrettage pressure of 200 MPa and an operating pressure of 180 MPa, a reduction of 15.7% in the maximum stress level has been achieved. It has been shown by them that the analysis of autofrettage is useful for improving the fatigue life of the cylinder by reducing the Von Mises stresses. They have run theoretical and FEA simulations to give a better understanding of the advantages of determining the residual stresses and their effect on the stress distribution. The Von Mises and Tresca Yield criteria have been used by them to calculate the theoretical maximum and minimum pressure that needs to be applied during the autofrettage process and compared with FEM results. During the study of stress distribution, it has been assumed by them that the thick-walled cylinder has withstood a uniform internal pressure, while the surrounding pressure has been considered a constant value. The corresponding equations for optimum autofrettage pressure have been used by them to determine the minimum and maximum autofrettage pressures. They have also demonstrated that, when loads were modelled in ANSYS(FEA), residual stresses were carried forward to all load phases.

Gennadiy Lvov et al. (2014) have used the Continuum damage mechanics approach for the analysis of the autofrettage process. Numerical results for the plane-strain case have been obtained by them using the finite-element method. The process of residual stress generation in a thick-walled cylinder has been investigated by them, considering temperature strain. The Prandtl-Reuss model has been used by them for plastic yielding of isentropic material. Theoretical and experimental results have been compared by them, showing a significant difference in residual stresses on the inner bore. The autofrettage thick-walled pipe has been suggested to be used as a part of the whole construction by them. Numerical solutions have been obtained by them using the finite element method, with the material model taking kinematical hardening and the ideal Bauschinger effect into account. Analytical and finite-element analysis have been used by them to find that the residual stress incorporating the Bauschinger effect at the inner bore is smaller than for isentropic hardening. The Ansys finite element software has been used by them to perform the numerical study. A plane model of the cylinder in Ansys with two-dimensional PLANE42 elements has been constructed by them. It has been concluded by them that the finite element method of the autofrettage thick-walled

tube calculates the influence of damage. A numerical procedure has been used by them to compare the residual hoop stress value with and without the material damage influence.

S. P. Pawar et al. (2015) have shown the study of distribution of thermal stresses for different values of the powers of the module of elasticity and varying power law index of heat generation. Material properties and heat generation have been assumed, with a function of the sphere and Poisson's ratio being constant. An attempt has been made to study the quasi-static thermal stresses based on uncoupled thermoelasticity for an FGM hollow thick sphere with non-uniform internal heat generation, which is a function of the radial position. The variation in the thermal stresses in the presence of a variable heat source, which varies from the inner to the outer surface, has been observed. It has also been observed that in the presence of the source in the present form, the temperature increases as the power law index decreases. They have illustrated results numerically and graphically.

Ruilin Zhu et al. (2017) have investigated the characteristics of stresses in cylinders subjected to internal pressure according to the maximum distortion strain energy theory and obtained a set of simplified equations for residual stresses and total stresses. The safe optimum load-bearing conditions for autofrettaged cylinders have been identified by them. They intended to investigate the varying tendency and distribution laws of stresses in autofrettaged cylinders in order to provide the theoretical basis for the design of high-pressure apparatus.

Marina Rynkovskaya et al. (2019) have considered three main end conditions plane strain, closed-end and open-end conditions. An elastic, perfectly plastic material model has been considered by them in the plane strain condition, which has been extended for closed-end tubes. A theory has also been proposed by them for the free end condition, where the Tresca yield criterion has been used, and the solution has been found by a finite difference method. They took into account an open-ended cylinder and assumed that the generalized Hooke's law connects the elastic stress and strain. They have suggested that a numerical technique is necessary to solve a linear differential equation. They have put out a theoretical solution for the distribution of residual stresses and strains in an open-ended, thick-walled cylinder that has been subjected to internal pressure and then unloaded. A common type of anisotropy, polar ortotrophy of elastic and plastic properties, has been concentrated on by them. The elastic response of the cylinder has been controlled by the generalized Hooke's law and the plastic response by the Tsai-Hill yield criterion and its associated flow rule. They have said that the solution can be directly applied to the study and design of the autofrettage process.

Ritu. J. Singh et al. (2019) have observed that anisotropy in the material properties may result due to manufacturing processes like extrusion or pilgering. They have mentioned that a thick cylinder made from Zr 2.5% Nb has been loaded till the elasto-plastic interface is achieved and then unloaded to study the effect of anisotropy on the development of residual stresses. Two material models have been considered in the analysis, i.e., isotropic and anisotropic plastic behavior. The effect of anisotropy on the residual stress has been investigated by them. Finite elements have been extensively used to verify the analytical solutions and to propose modifications to analytical solutions. It has been seen by them that the effect of anisotropy on the residual stress in the roll expanded joint may be an important parameter and needs to be investigated. The commercial FE software ABAQUS has been used by them for modeling the autofrettaged thick cylinder considering $1/4^{th}$ symmetry. During the autofrettage, it has been observed by them that the residual stress obtained for the two-material model was substantially different. It has been noted by them that for anisotropic material properties as per the hills yield criterion, yielding initiates at a higher pressure compared to the isotropic material model. For a given expansion pressure, this results in less plastification of the cylinder than in the isotropic case, which lowers residual stresses.

Guiqin Li et al. (2021) have carried out a stress analysis, where the UHP vessel has been operated under high pressure and stress. The reinforced UHP vessel has been divided into elastic and plastic parts for their analysis, and the best autofrettaged pressure has been obtained under certain working pressure. The Shigley approximation method has been used by them for fatigue life prediction. In this work, the fatigue life of the autofrettaged UHP vessel has been accurately predicted. Ordinary containers and autofrettaged containers have been compared by them, and it has been concluded that the fatigue life of autofrettaged containers can be significantly improved.

S.C. Mondal et al. (2017) have noted that the elastic-plastic stress distribution subjected to thermal load has been evaluated. Residual stress prediction has been used on uniaxial loading-unloading stress of an elastic perfectly plastic material model. The feasibility of centrifugal and centripetal autofrettage has been discussed and compared. The behavior of thick-walled spherical and cylindrical vessels under thermal and mechanical stresses has been considered. An exact solution has been obtained for the stress distribution in a thick-walled sphere made of elastic-perfectly plastic material under a steady state and radial temperature gradient. The approximate solution with negligible elastic strain has also been examined. The onset of yield in thick-walled spherical vessels for various combinations of temperature, pressure, and various

radius ratios has also been studied. Finite element analysis with ANSYS has been performed on a spherical vessel for thermal autofrettage and compared with mechanical autofrettage. A finite element 2-D model of an autofrettaged sphere has been constructed. Centripetal thermal residual stress has been obtained from the analytical elastic perfectly plastic model and compared with the results of the 2D FE model in ANSYS. It has been observed that autofrettage stresses show excellent agreement. It has also been observed that there is a negligible difference between the stresses obtained by analytical expressions and the FE model.

Mengjun ZHAO et al. (2005) have introduced an internal autofrettaged cylinder with interlayer pressure (ACCIP), to improve the bearing pressure capacity of ultrahigh-pressure apparatus. Its derivation and the analytical model for the ACCIP structure have been presented by them. In this work, it has been shown that the ACCIP method has enhanced the bearing pressure of the apparatus. It has been suggested by them that ACCIP be set up and the analytical model be presented to increase the elastic-limit capacity and obtain the optimum radial dimension of the ultra-high pressure apparatus. It has been noted by them that the limit workload has been close to 1.5 times the yield strength σ_y by using the ACCIP method. It has been concluded by them that the calculation of the stresses has been based on the ideal conditions and the calculated results have revealed that the plastic limit workload P_w can be as high as 1.5 times the yielding strength σ_y, which is much larger than those of the shrink-fit vessel and the autofrettaged cylinder. It has been studied and indicated by them that there has been an optimum interlayer pressure when the total radius ratio is used as the minimum. It has been concluded by them that the ACCIP method can both increase the elastic-limit workload of ultrahigh-pressure apparatus and optimize its structure.

The impact of internal pressure in a hollow spherical shell with functional gradations is theoretically examined in this research. It is presumptuous that the material properties in the graded direction follow a power law distribution. The Navier and heat conduction equations are directly solved in order to determine the impact of internal pressure and temperature on the design of pressure vessels. The pressure variation and mechanical stress distribution, such as radial stress distribution and hoop stress distribution along the radial direction, are provided in sequential order. In the result and discussion section, the radial distribution of temperature has also been shown. The study also aims to understand the influence of autofrettage on stress distribution and load bearing capacity in thick spherical shells. Analytical equations, derived from the Maximum Shear Stress theory and Distortion Energy theory, determine the optimal radius of the elastic-plastic juncture $C_{opt,}$ in autofrettage. Results reveal that autofrettage

increases internal pressure, enhancing the shell's capability to withstand higher pressures. Additionally, it has been established that temperatures rise as the power law index value rises. Therefore, it is possible to draw the conclusion that a material with a lower power law index benefits from the formation of lower thermal stress.

CHAPTER 2

2. MATHEMATICAL FORMULATION

Consider a spherical shell with an inner and outer radius of a and b, respectively, that is under a constant internal pressure of p, as shown in Figure 2.1.

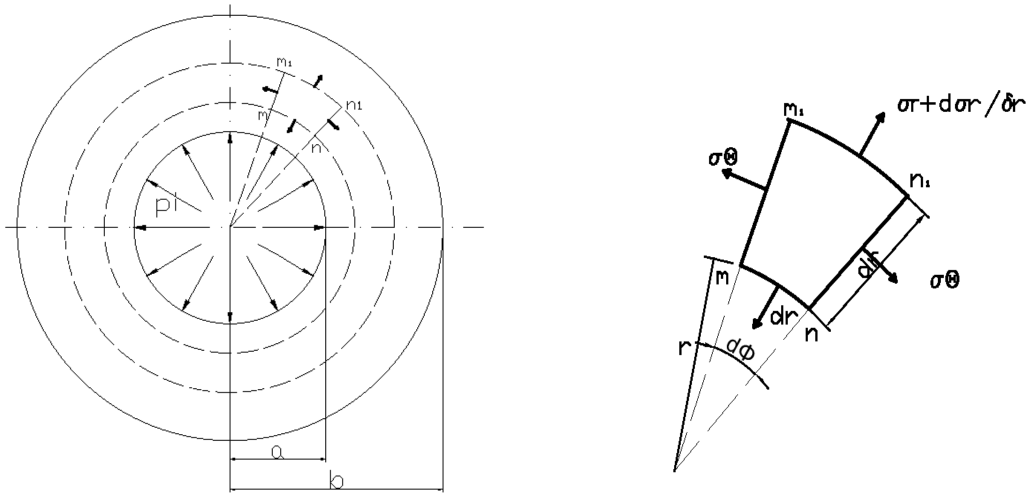

Figure 1: Spherical Shell Under Internal Pressure

2.1 Study of influence of autofrettage on a spherical shell:

The equivalent stress, as derived from the distortion energy theory, is as follows:

$$\sigma_{eq}^{iv} = \left[\frac{1}{2}\{(\sigma_\theta - \sigma_\emptyset)^2 + (\sigma_\emptyset - \sigma_r)^2 + (\sigma_r - \sigma_\theta)^2\}\right]^{1/2} \ldots\ldots\ldots\ldots\ldots\ldots (1)$$

Where,

$\sigma_\emptyset$, σ_r, σ_θ are represented as Radial, hoop, and axial stress, respectively.

Superscript "iv" represents quantity based on the Von Mises strength theory.

σ_{eq} represents equivalent stress at r = c.

Because of the symmetry of the spherical shell $\sigma_\theta = \sigma_\emptyset$ so, substituting $\sigma_\theta = \sigma_\emptyset$ into the equation (1), we obtain

$$\sigma_{eq} = \sigma_\theta - \sigma_r = \sigma_\emptyset - \sigma_r \ldots\ldots\ldots\ldots\ldots\ldots (2)$$

From this relation and the Distortion Energy Theory, we obtain the intended result.

2.1.1 Determination of the optimum radius of the elastic-plastic junction, c_{opt}:

The stress equation of equilibrium can be derived easily. Consider a spherical element of thickness Δr at a distance of r, subtending a small angle 2θ at the centre. Because of spherical

symmetry $\sigma_\theta = \sigma_\emptyset$, for equilibrium in the radial direction, the equilibrium equation ignores the body forces.

$\frac{d\sigma_r}{dr} = \frac{2(\sigma_\emptyset - \sigma_\theta)}{r}$ ……. (3)

Again, the maximum Distortion energy theory for the spherical shell from equation (2) becomes

$\sigma_y = \sigma_\theta - \sigma_r = \sigma_\emptyset - \sigma_r$ ……..…..... (4)

Where,

σ_y represents Yield strength

Combining equations (3) and (4) and after integrating we have,

$\sigma_r = 2\sigma_y \ln r + c_1$ ……..……... (5)

The stress in the elastic spherical shell for the internal pressure p is

$\sigma_r^e = \frac{p}{k^3-1}\left(\frac{b^3}{r^3} - 1\right)$ ……..……..…… (6)

$\sigma_\theta^e = \sigma_\emptyset^e = \frac{p}{k^3-1}\left(\frac{b^3}{2r^3} + 1\right)$ ……..…….. (7)

Where,

K = $\frac{b}{a}$, the ratio of inside to outside radius

A spherical shell's inside radius, elastic-plastic junction radius, and outer radius are represented by a, c, and b.

Putting the value of σ_r^e; as from equation (6), at the elastic-plastic juncture, the plastic stress and elastic stress are equal, and also applying the boundary condition, the plastic stress in the region as a ≤ r ≤ c are

$\sigma_r^p = -\frac{2\sigma_y}{3}\left(1 - \frac{c^3}{b^3} + \ln\frac{c^3}{r^3}\right)$ ……... (8)

And from equation (4)

$\sigma_\theta^p = \sigma_\emptyset^p = \frac{2\sigma_y}{3}\left(\frac{1}{2} + \frac{c^3}{b^3} + \ln\frac{c^3}{r^3}\right)$ ……..…..… (9)

The initial pressure p' must be utilised to create plastic flow in the wall up to the depth corresponding to the radius r = c and elastic flow from r = c to the outside surface r = b. Now that we have the value r = a, we can determine the initial pressure's magnitude.

$$p' = -\sigma_r^p = \frac{2\sigma_y}{3}\left(1 - \frac{c^3}{b^3} + \ln\frac{c^3}{r^3}\right) \quad \text{(10)}$$

Now after the partial yielding of the shell wall, the inner pressure p' is removed, and some residual stress will remain in the wall of the spherical shell. The inner wall section where the plastic deformation took place does not return back to its original dimension. The elastic movement from the shell's outer to inner surfaces occurs when internal pressure is released (p'). Therefore, after removing the internal pressure p', the elastic equations are used to calculate the stress during elastic flow from the outer surface to the inner surface. So, the elastic stresses after the removal of the internal pressure in the region $a \leq r \leq b$ is

$$\sigma_r^e = \frac{2\sigma_y}{3(k^3-1)}\left(\frac{b^3}{r^3} - 1\right)\left[1 - \frac{c^3}{b^3} + \ln\frac{c^3}{a^3}\right] \quad \text{(11)}$$

$$\sigma_\theta^e = \sigma_\emptyset^e = \frac{2\sigma_y}{3(k^3-1)}\left(\frac{b^3}{2r^3} + 1\right)\left[1 - \frac{c^3}{b^3} + \ln\frac{c^3}{a^3}\right] \quad \text{(12)}$$

So, the residual stresses persist after removing the internal pressure in the region $a \leq r \leq c$,

$$\sigma_r' = \frac{2\sigma_y}{3(k^3-1)}\left(\frac{b^3}{r^3} - 1\right)\left[1 - \frac{c^3}{b^3} + \ln\frac{c^3}{a^3}\right] - \frac{2\sigma_y}{3}\left[1 - \frac{c^3}{b^3} + \ln\frac{c^3}{r^3}\right] \quad \text{(13)}$$

$$\sigma_\theta' = \sigma_\emptyset' = \frac{2\sigma_y}{3(k^3-1)}\left(\frac{b^3}{2r^3} + 1\right)\left[1 - \frac{c^3}{b^3} + \ln\frac{c^3}{a^3}\right] + \left[\frac{1}{2} + \frac{c^3}{b^3} + \ln\frac{c^3}{r^3}\right] \quad \text{(14)}$$

Now the residual stresses at the shell surface r = c, which separate the elastic and plastic zone from the equation (13) and (14)

$$[\sigma_r']_{r=c} = \frac{2\sigma_y}{3}\left(1 - \frac{c^3}{b^3}\right)\left[\frac{b^3}{r^3}\left(1 - \frac{c^3}{b^3} + \ln\frac{c^3}{a^3}\right)\frac{1}{k^3-1} - 1\right] \quad \text{(15)}$$

$$[\sigma_\theta']_{r=c} = [\sigma_\emptyset']_{r=c} = \frac{2\sigma_y}{3}\left(\frac{1}{2} + \frac{c^3}{b^3}\right)\left[\frac{b^3}{c^3}\left(1 - \frac{c^3}{b^3} + \ln\frac{c^3}{a^3}\right)\frac{1}{k^3-1} + 1\right] \quad \text{(16)}$$

We can determine the total stresses in an autofrettage-treated spherical shell at r = c by adding the corresponding stresses in equations (6), (7), and (15), (16) respectively.

$$\sigma_r^T = [\sigma_r']_{r=c} + \sigma_r^p \quad \text{(17)}$$

$$\sigma_\theta^T = \sigma_\emptyset^T = [\sigma_\theta']_{r=c} + \sigma_P^\theta = [\sigma_\emptyset']_{r=c} + \sigma_\emptyset^p \quad \text{(18)}$$

Where,

The superscripts P and T refer to total stress and pressure-related stress, respectively.

Substituting equations (17) and (18) into equation (2), at r = c, we find the equivalent stress.

$$\sigma_{eq}^{iv} = \sigma_y + \frac{\sigma_y}{k^3-1}\left[\frac{5}{3} - \frac{4c^3}{3b^3} + \frac{4}{3}\ln\frac{c^3}{a^3} - \frac{b^3}{3c^3} - \frac{b^3}{3c^3}\ln\frac{c^3}{a^3}\right] + \frac{p}{k^3-1}\left(\frac{3b^3}{2c^3}\right) \ldots\ldots\ldots\ldots\ldots\ldots\ldots\ldots (19)$$

Letting,

$$\frac{d\sigma_{eq}^{iv}}{dc} = 0$$

$$\left(\frac{c}{b}\right)^6 - \left(\frac{c}{b}\right)^3 - \frac{3}{4}\ln\frac{c}{a} + \frac{9}{8}\left(\frac{p}{\sigma_y}\right) = 0$$

As c/b is very small so, neglecting the higher order terms we obtain:

$$c_{opt} = a\exp\left(\frac{3p}{2\sigma_y}\right) \ldots\ldots\ldots\ldots\ldots\ldots\ldots\ldots\ldots\ldots\ldots\ldots\ldots\ldots\ldots\ldots\ldots\ldots\ldots\ldots\ldots (20)$$

Where,

Subscript “opt” represents the optimum quantity

At c = c_{opt},

$$\frac{d\sigma_{eq}^{iv}}{dc} > 0$$

That means the σ_{eq}^{iv} at $c = c_{opt}$ is minimal, the optimum radius of the elastic-plastic junction consequently becomes c_{opt}.

By equation (20): Direct representation of P and σ_y effect on c_{opt} is possible. For example, in order to enhance the spherical shell's load bearing ability, c_{opt} should be higher if P is high (the thickness of the shell's wall will be high); while σ_y, is large, c_{opt} may be small, this is because of the material's great σ_y and high load-bearing capacity. P_y entire yield internal pressure of the spherical shell can be obtained directly from equation (20). It needs only to let.

$$p_y^{iv} = \frac{2}{3}\sigma_y \ln k \ldots\ldots\ldots\ldots\ldots\ldots\ldots\ldots\ldots\ldots\ldots\ldots\ldots\ldots\ldots\ldots\ldots\ldots\ldots\ldots\ldots (21)$$

Thus, it is observed that by using equation (20), we can obtain c_{opt} more accurately, this is the most reasonable as well as simple and applicable method.

2.1.2 Influence of autofrettage on a spherical shell:

From equation (8), We know that autofrettage can't increase σ_y of a spherical shell from equation (8). But it can make a spherical shell's elastic strength better. The maximum allowed

pressure for a spherical shell treated with autofrettage is given by equation (21), whereas the maximum permitted pressure for a shell without autofrettage treatment is given by

$p_e^{iv} = \frac{2\sigma_y}{3}\frac{k^3-1}{k^3}$ ……..…….... (22)

$p_e^{iv} = \frac{2\sigma_y}{3}$ (k – α) …….…….....…. (23)

Where,

P_e represents the maximum internal pressure of the spherical shell that can contain elasticity.

From equation (21) and (22), we get

$\lambda = \frac{k^3 \ln k}{k^3-1} = \frac{p_y^{iv}}{p_e^{iv}}$ …….…….. (24)

2.1.3 Determination of optimum autofrettage pressure of a thick spherical shell:

The optimal autofrettage pressure, p_{aopt}, is the internal pressure that must be supplied before a spherical shell is used for production. c_{opt} is obtained by the surface of it yielding. We obtain autofrettage pressure using the Von Mises strength theory.

$p_a^{iv} = \frac{2\sigma_y}{3}\left(1 - \frac{c^3}{b^3} + \ln\frac{c^3}{r^3}\right)$ ……..……...…… (25)

Where,

P_a represents autofrettage pressure

Substituting equation (20) into the equation (25), we obtain:

$p_{aopt}^{iv} = \frac{2\sigma_y}{3}\left[1 - \frac{1}{k^3} exp\left(\frac{9p}{2\sigma_y}\right)\right]$ + 3p ……...… (26)

From equation (9), we obtain $1/k^3$ = 1-3p/$2\sigma_y$, therefore

$p_{aopt}^{iv} = \frac{2\sigma_y}{3}\left[1 - \left(1 - \frac{3p}{2\sigma_y}\right) exp\left(\frac{9p}{2\sigma_y}\right)\right]$ + 3p ……..……..… (27)

Figure 3.3 depicts the relationship between p_{aopt} and p. From this, we are able to determine that p_{aopt} must be a little larger than p in order for the wall of a spherical shell to yield.

2.2 Stress calculation considering thermal effect

Consider the shell is subjected to purely radial temperature variation, i.e. T is a function of 'r' alone. Because of symmetry, shear stresses are all zero and the normal stresses are such that $\sigma_{\emptyset} = \sigma_{\theta}$. Equation (1) from above can be also written as,

Considering the equilibrium in the radial direction,

$\frac{d(r^2\sigma_r)}{dr} - 2r\sigma_{\emptyset} = 0$ ……..…..... (28)

The stress-strain relations are,

$\varepsilon_r = \frac{1}{E}(\sigma_r - 2\mu\sigma_{\emptyset}) + \alpha T$ ……..…..…. (29)

$\varepsilon_{\emptyset} = \frac{1}{E}(\sigma_{\emptyset}(1-\mu) - \mu\sigma_r) + \alpha T$ ……...……...….... (30)

Now, Consider equation (29)

$\varepsilon_r = \frac{1}{E}(\sigma_r - 2\mu\sigma_{\emptyset}) + \alpha T$

$\varepsilon_r = \frac{\sigma r}{E} + \frac{2\mu\sigma_{\emptyset}}{E} + \frac{\alpha T}{E}$

$\varepsilon_r = \frac{\sigma r - 2\mu\sigma_{\emptyset} + \alpha T}{E}$

$E\varepsilon r = \sigma r - 2\mu\sigma_{\emptyset} + \alpha T$

$\alpha TE + \sigma_r - E\varepsilon r = 2\mu\sigma_{\emptyset}$

$\sigma_{\emptyset} = \frac{\alpha TE + \sigma_r - E\varepsilon_r}{2\mu}$ ……. (29.1)

Using equation (29.1) in equation (30)

$\varepsilon_{\emptyset} = \frac{1}{E}\frac{(\{\alpha ET + \sigma_r - E\varepsilon_r\}}{2\mu} - (1-\mu) - \mu\sigma_r + \alpha T$

$\varepsilon_{\emptyset} = \frac{1}{E}\frac{(\{\alpha ET + \sigma_r - E\varepsilon_r\}}{2\mu} - \mu\frac{(\{\alpha ET + \sigma_r - E\varepsilon_r\}}{2\mu} - \mu\sigma_r + \alpha T$

$\varepsilon_{\emptyset} = \frac{1}{E}\frac{(\{\alpha ET + \sigma_r - E\varepsilon_r\}}{2\mu} - \frac{(\{\alpha ET\mu + \mu\sigma_r - \mu E\varepsilon_r\}}{2\mu} - \mu\sigma_r + \alpha T$

$\varepsilon_{\emptyset} = \frac{1}{E}\frac{(\alpha ET + \sigma_r - E\varepsilon_r - \alpha ET\mu + \mu\sigma_r - E\mu\varepsilon_r - 2\mu^2\sigma_r)}{2\mu} + \alpha T$

$\varepsilon_{\emptyset} = \frac{\alpha ET + \sigma_r - E\varepsilon_r - \alpha ET\mu + \mu\sigma_r - E\mu\varepsilon_r - 2\mu^2\sigma_r + 2E\mu\alpha T}{2E\mu}$

$$\varepsilon_{\emptyset} = \frac{\alpha ET + \alpha ET\mu + 2E\mu\alpha T - E\varepsilon_r + E\mu\varepsilon_r + \sigma_r - \mu\sigma_r - 2\mu^2\sigma_r}{2E\mu}$$

$$\varepsilon_{\emptyset} = \frac{\alpha ET + \alpha ET\mu - E\varepsilon_r + E\mu\varepsilon_r + \sigma_r - \mu\sigma_r - 2\mu^2\sigma_r}{2E\mu}$$

$$\varepsilon_{\emptyset} = \frac{E(\alpha T - \alpha T\mu - \varepsilon_r + \mu\varepsilon_r) + \sigma_r\left(1 - \mu - 2\mu^2\right)}{2E\mu}$$

$$\varepsilon_{\emptyset} = \frac{E(\alpha T - \alpha T\mu - \varepsilon_r + \mu\varepsilon_r)}{2E\mu} + \frac{\sigma_r\left(1 - \mu - 2\mu^2\right)}{2E\mu}$$

$$\varepsilon_{\emptyset} = \frac{\alpha T\left((1+\mu) - \varepsilon_r(1-\mu)\right)}{2\mu} = \frac{\sigma_r\left(1-\mu-2\mu^2\right)}{2E\mu}$$

$$= \frac{\sigma_r\left(1-\mu-2\mu^2\right)}{2E\mu} = \frac{2\mu\varepsilon_{\emptyset} - (\alpha T(1+\mu) + \varepsilon_r(1-\mu))}{2\mu}$$

$$= \frac{\sigma_r\left(1-\mu-2\mu^2\right)}{2E} = \frac{2\mu\varepsilon_{\emptyset} - (\alpha T(1+\mu) - \varepsilon_r(1-\mu))}{2}$$

$$\sigma_r = \frac{E(2\mu\varepsilon\emptyset - \alpha T(1+\mu) + \varepsilon_r(1-\mu))}{1-\mu-2\mu^2}$$

$$\sigma_r = \frac{E}{1-\mu-2\mu^2}\left((1-\mu)\varepsilon_r + 2\mu\varepsilon_{\emptyset} - (1+\mu)\alpha T\right)$$

$$\sigma_r = \frac{E}{(1-2\mu)(1+\mu)}\left[(1-\mu)\varepsilon r + 2\mu\varepsilon_{\emptyset} - (1+\mu)\alpha T\right] \quad \text{.. (31)}$$

Now, putting the value of σr from equation (31) into equation (29), we get

$$\varepsilon_r = \frac{1}{E}\frac{E}{(1-2\mu)(1+\mu)}\left[(1-\mu)\varepsilon_r + 2\mu\varepsilon_{\emptyset} - (1+\mu)\alpha T\right] - 2\mu\sigma_{\emptyset} + \alpha T$$

$$\varepsilon_r = \frac{(1-\mu)\varepsilon_r + 2\mu\varepsilon_{\emptyset} - (1+\mu)\alpha T}{(1-2\mu)-(1+\mu)} - \frac{2\mu\sigma_{\emptyset}}{E} + \alpha T$$

$$\varepsilon_r = \frac{E\left[(1-\mu)\varepsilon_r + 2\mu\varepsilon_{\emptyset} - (1+\mu)\alpha T\right] - 2\mu\sigma\emptyset\left[(1-2\mu)(1+\mu)\right] + \alpha TE(1-2\mu)(1+\mu)}{E(1-2\mu)-(1+\mu)}$$

$$\begin{aligned} E(1-2\mu) - (1+\mu)\varepsilon_r \\ &= E[(1-\mu)\varepsilon_r + 2\mu\varepsilon_{\emptyset} - (1+\mu)\alpha T] - 2\mu\sigma_{\emptyset}\,[(1-2\mu)(1+\mu)] \\ &+ \alpha TE(1-2\mu)(1+\mu) \end{aligned}$$

$$2\mu\sigma_{\emptyset}\,[(1-2\mu)(1+\mu)] = E[(1-\mu)\varepsilon_r + 2\mu\varepsilon_{\emptyset} - (1+\mu)\alpha T] - [E(1-2\mu) - (1+\mu)\varepsilon_r] + \alpha TE(1-2\mu)(1+\mu)$$

$$2\mu\sigma_{\emptyset}\,[(1-2\mu)(1+\mu)] = E[(1-\mu)\varepsilon_r + 2\mu\varepsilon_{\emptyset} - (1+\mu)\alpha T] - [(1-2\mu) - (1+\mu)\varepsilon_r] + \alpha T(1-2\mu)(1+\mu)$$

$$\sigma_{\emptyset} = \frac{E}{2\mu[(1-2\mu)(1+\mu)]}[(\varepsilon_r - \mu\varepsilon_r + 2\mu\varepsilon_{\emptyset} - \alpha T - \mu\alpha T - [\varepsilon_r - \mu\varepsilon_r + 2\mu^2\varepsilon_r] + (\alpha T - \mu\alpha T - 2\mu^2\alpha T)]$$

$$\sigma_{\emptyset} = \frac{E}{2\mu[(1-2\mu)(1+\mu)]}[(\varepsilon_r - \mu\varepsilon r + 2\mu\varepsilon_{\emptyset} - \alpha T - \mu\alpha T - \varepsilon_r + \mu\varepsilon_r + 2\mu^2\varepsilon_r + \alpha T - \mu\alpha T - 2\mu^2\alpha T)]$$

$$\sigma_{\emptyset} = \frac{E}{(1-2\mu)(1+\mu)}\left(\frac{2\mu\varepsilon_{\emptyset} - 2\mu\alpha T + 2\mu^2\varepsilon_r - 2\mu^2\alpha T}{2\mu}\right)$$

$$\sigma_{\emptyset} = \frac{E}{(1-2\mu)(1+\mu)}\left(\frac{2\mu(\varepsilon_{\emptyset} - \alpha T + \mu\varepsilon_r - \alpha\mu T}{2\mu}\right)$$

$$\sigma_{\emptyset} = \frac{E}{(1-2\mu)(1+\mu)}\,[\varepsilon_{\emptyset} - \alpha T(1+\mu) + \mu\varepsilon_r] \quad \text{..... (32)}$$

From strain displacement relations, we have

$$\varepsilon_r = \frac{dur}{dr}\,;\quad \varepsilon_{\emptyset} = \varepsilon_{\theta} = \frac{Ur}{r} \quad \text{..... (33)}$$

Now, Putting the value of εr & $\varepsilon_{\emptyset}$ in equation (31)

$$\sigma_r = \frac{E}{(1-2\mu)(1+\mu)}\left[(1-\mu)\frac{dur}{dr} + 2\mu\,\frac{Ur}{r} - (1+\mu)\alpha T\right] \quad \text{..... (34)}$$

Also,

$$\sigma_{\emptyset} = \frac{E}{(1-2\mu)(1+\mu)}\,[\mu\varepsilon_r + \varepsilon_{\emptyset} - (1+\mu)\alpha T]$$

Putting value of $\varepsilon_{\emptyset}$ & ε_r in equation (32)

$$\sigma_{\emptyset} = \frac{E}{(1-2\mu)(1+\mu)}\left[\mu\,\frac{dur}{dr} + \frac{Ur}{r} - (1+\mu)\alpha T\right] \quad \text{..... (35)}$$

Now, λ & G are lame's coefficient related to the modulus of elasticity E and Poisson's ratio μ as,

$$\lambda = \frac{\mu E}{(1+\mu)(1-2\mu)}\,;\ \mathrm{G} = \frac{E}{2(1+\mu)} \quad \text{..... (36)}$$

Now, equation (34) & (35) reduces to,

$$\sigma_r = (\lambda + 2\mathrm{G})\varepsilon_r + 2\lambda\varepsilon_{\emptyset} - (3\lambda + 2\mathrm{G})\alpha T \quad \text{..... (37)}$$

Equation (34) reduces to,

$$\sigma_r = \frac{E}{(1-2\mu)(1+\mu)}\left((1-\mu)\frac{dur}{dr} + 2\mu\,\frac{Ur}{r} - (1+\mu)\alpha T\right)$$

1st term,

$$\lambda + 2G = \frac{\mu E}{(1+\mu)(1-2\mu)} + \frac{E}{2(1+\mu)}$$

$$\frac{\mu E+(1-2\mu)E}{(1+\mu)(1-2\mu)} = \frac{\mu E+E-2\mu E}{(1+\mu)(1-2\mu)}$$

$$\frac{E-\mu E}{(1+\mu)(1-2\mu)} = \frac{E(1-\mu)}{(1+\mu)(1-2\mu)}$$

2nd term,

$$2\lambda\varepsilon_\emptyset = 2\mu\varepsilon_\emptyset \times \frac{E}{(1-2\mu)(1+\mu)}$$

$$\frac{2\mu E}{(1-2\mu)(1+\mu)}\,\varepsilon_\emptyset = 2\lambda\varepsilon_\emptyset$$

3rd term,

$$3\lambda + 2G = \frac{3\mu E}{(1+\mu)(1-2\mu)} + \frac{E}{(1+\mu)} = \frac{3\mu E+E(1-2\mu)}{(1+\mu)(1-2\mu)}$$

$$= \frac{3\mu E+E-2\mu E}{(1+\mu)(1-2\mu)}$$

$$= \frac{\mu E+E}{(1+\mu)(1-2\mu)}$$

$$= \frac{E(1+\mu)}{(1+\mu)(1-2\mu)}$$

Similarly,

$$\sigma_\emptyset = (2\lambda + 2G)\,\varepsilon_\emptyset + \lambda\varepsilon r - (3\lambda + 2G)\alpha T \quad \text{……..…… (38)}$$

Equations (35) reduce to,

$$\sigma_\emptyset = \frac{E}{(1-2\mu)(1+\mu)}\left[\mu\,\frac{dur}{dr} + \frac{Ur}{r} - (1+\mu)\alpha T\right]$$

1st term,

$$(2\lambda + 2G)\varepsilon_\emptyset = \left(\frac{2\mu E}{(1+\mu)(1-2\mu)} + \frac{2E}{2(1+\mu)}\right)\varepsilon_\emptyset$$

$$\frac{2\mu E+(1-2\mu)E}{(1+\mu)(1-2\mu)} = \frac{2\mu E+ E- 2\mu E}{(1+\mu)(1-2\mu)}$$

$$= \frac{E(1-\mu)}{(1+\mu)(1-2\mu)}$$

2nd term,

$\lambda\varepsilon r = \mu\varepsilon_r \times \frac{E}{(1-2\mu)(1+\mu)}$

$$\frac{\mu E}{(1-2\mu)(1+\mu)}\ \varepsilon_r = \lambda\varepsilon r$$

3rd term,

$(3\lambda + 2G)\alpha T = \frac{3\mu E}{(1-2\mu)(1+\mu)} + \frac{2E}{2(1+\mu)}$

$$= \frac{3\mu E+E(1-2\mu)}{(1-2\mu)(1+\mu)}$$

$$= \frac{3\mu E+E- 2\mu E}{(1-2\mu)(1+\mu)} = \frac{\mu E+E}{(1-2\mu)(1+\mu)}$$

$$= \frac{E(1+\mu)}{(1-2\mu)(1+\mu)}$$

Now,

E(r) = $E_o r^{m_1}$ and $\acute{\alpha} = \acute{\alpha} r^{m_2}$ ……..……... (39)

Where, E_o = constant

$\acute{\alpha_O}$ = constant

m_1 & m_2 = Power law indices

Now in equation (34), replace E with $E_o r^{m1}$ and in equation (35) replace α with $\acute{\alpha_O} r^{m2}$

Equation (34) and (35) becomes,

$\sigma_r = \frac{E_o r^{m1}}{(1-2\mu)(1+\mu)} \left[(1-\mu)\frac{dur}{dr} + 2\mu\ \frac{Ur}{r} - (1+\mu)\acute{\alpha_O} r^{m2} T)\right]$ ……..….. (40)

$\sigma_\emptyset = \frac{E_o r^{m1}}{(1-2\mu)(1+\mu)} \left[\frac{Ur}{dr} + \mu\frac{dur}{r} - (1+\mu)\acute{\alpha_O} r^{m2} T\right]$ ……..….. (41)

Now, putting the values from the equation σ_r and $\sigma_\emptyset$ From equation (40) and (41) into equation (28), we obtain

$$U_r" + (m_1 + 2)\frac{U_{r'}}{r} + 2\left(\frac{\mu m_1}{1-\mu} + 1\right)\frac{U_r}{r^2} = \frac{1+\mu}{1-\mu}\alpha_o\left((m_1 + m_2)r^{m2+1}\,T + r^{m2+2}\,T'\right) \text{…….. (42)}$$

2.3 Heat Conduction Calculation

The heat conduction equation in the steady state condition for a one-dimensional problem in polar coordinates and thermal boundary conditions for an FGM hollow sphere are given, respectively as

$$\frac{1}{r^2}[r^2k(r)T'(r)]' = 0; C_{11}T(a) + C_{22}T'(a) = f_1$$

C_{21}T(b) + $C_{22}T'(b) = f_2, a \le r \le b$ …….……..……. (43)

Where a and b are the inside and outside radii of the shell

k=k(r) represents the thermal conduction coefficient

C_{ij} are constant thermal parameters related to the conduction and convection coefficients.

It is assumed that the non-homogeneous thermal conduction coefficient k(r) is a power function of r as

K(r) = $K_0 r^{m_3}$ ……..…..……...…. (44)

Where, K_0 and m_3 are the material parameters. Using equation (44), the heat conduction equation becomes

$\frac{1}{r^2}[k_0 r^{m_3+2}T'(r)]' = 0$ ……...…… (45)

Integrating once equation (45)

$\int[k_0 r^{m_3+2}T'(r)]' = 0$

$k_0 r^{m_3+2}T'(r) = 0$

Again integrating, we get

$k_0 r^{m_3+2}T'(r) + A_1 = 0$

$T'(r) = \frac{-A_1}{r^{(m_3+2)}}$ ……..……...……..…. (46)

We need to perform integration twice with respect to r

Let's start by rearranging the equation

$\frac{(Kor^{(m_3+2)}T'(r))}{r^2} = 0$

Integrating both sides with respect to r once, we get

$\frac{(Kor^{(m_3+2)}T'(r))}{r^2} = A_1$

Where A_1 is the constant of integration,

Simplifying this expression, we get

$T'(r) = \frac{A_1 r^{(-m_3-2)}}{K}$

Integrating both sides again w.r.t r, we get

$T(r) = \frac{-A_1}{(m_3+1)} r^{(-m_3-1)} + A_2$

Where A_2 is another constant of integration,

The final solution is:

T(r) = $\frac{-A_1}{(m_3+1)} r^{-(m_3+1)} + A_2$ …….……..…… (47)

Using the below boundary conditions to determine the constant A_1 & A_2,

$C_{11}T(a) + C_{22}T'(a) = f_1$ …….…… (48)

C_{21}T(b) + $C_{22}T'(b) = f_2, a \leq r \leq b$ ……... (49)

To determine constant A_1, we will use the boundary conditions (48) & (49),

T(a): Represents the temperature at the inner radius of the sphere (r = a).

T(b): Represents the temperature at the outer radius of the sphere (r = b).

T'(a): Denotes the derivative of temperature T with respect to r evaluated at r = a.

T'(b): Denotes the derivative of temperature T with respect to r evaluated at r = b.

Substituting equation (46) & (47) into equation (48) & (49), we get (50) & (51)

$C_{11}\left(\frac{-A_1}{m_3+1}a^{-(m_3+1)}+A_2\right)-\frac{A_1C_{22}}{(a^{(m_3+2)})}=f_1$ ……..….. (50)

$C_{21}\left(\frac{-A_1}{m_3+1}b^{-(m_3+1)}+A_2\right)-\frac{A_1C_{22}}{(b^{(m_3+2)})}=f_2$ …….…. (51)

Now, we need to solve above two equations for A_1, we can simplify these equations by multiplying equation (50) by C_{21} and equation (51) by C_{11} and then subtracting the both equations.

$$C_{21}C_{11}\left(\frac{-A_1}{(m_3+1)a^{-(m_3+1)}}+A_2\right)-\frac{C_{11}\,A_1C_{22}}{a^{(m_3+2)}}-\frac{C_{21}\,A_1C_{22}}{b^{(m_3+2)}}+$$

$$C_{11}C_{21}\left(\frac{-A_1}{(m_3+1)b^{-(m_3+1)}}+A_2\right)=f_1C_{21}-\ f_2C_{11}$$

Simplifying this equation and grouping terms containing A_1, we get

$$A_1=\frac{(C_{21}f_1-C_{11}f_2)K_0}{C_{21}\left(C_{12}a^{-(m_3+2)}\frac{C_{11}a^{(-m_3+1)}}{m_3+1}\right)-C_{11}\left(C_{12}a^{-(m_3+2)}\frac{C_{11}a^{(-m_3+1)}}{m_3+1}\right)}$$ ……..….. (52)

To solve for A_2 using the given boundary condition, we need to use equations (43) & (47)

First, we can differentiate equation (47) with respect to r to obtain $T'(r)$:

$$T'(r)=\frac{A_1}{(m_3+1)}(m_3+1)r^{(-m_3-2)}$$

Substituting this expression for $T'(r)$ into the left-hand side of equation (43) and simplifying, we obtain:

$$\frac{(r^2K(r)A_1)}{m_3+1}(-m-2)r^{(-m_3-3)}=0$$

Solving for A_1, we obtain equation (52) given above

Next, we use equation (47) to obtain the expression for T(a) and T'(a):

$$T_a=\frac{-A_1}{(m_3+1)}a^{(-m_3-1)}+A_2$$

$$T'_a=\frac{A_1}{m_3+1}(m_3+1)a^{(-m_3-2)}$$

We can then use the boundary condition $C_{11}T(a)+C_{22}T'(a)=\ f_1$ to obtain an expression for A_2

$$C_{11}\left(\frac{-A_1}{m_3+1}a^{-(m_3-1)}+A_2\right)+C_{22}\left(\frac{A_1}{m_3+1}-(m_3+1)a^{(-m_3-2)}\right)=f_1$$

Simplifying this equation and solving for A_2

$$A_2 = \frac{f_2\left(C_{12}a^{-(m_3+2)}\frac{C_{11}a^{(-m_3+1)}}{m_3+1}\right) - f_1\left(C_{12}a^{-(m_3+2)}\frac{C_{11}a^{(-m_3+1)}}{m_3+1}\right)}{C_{21}\left(C_{12}a^{-(m_3+2)}\frac{C_{11}a^{(-m_3+1)}}{m_3+1}\right) - C_{11}\left(C_{12}a^{-(m_3+2)}\frac{C_{11}a^{(-m_3+1)}}{m_3+1}\right)} \quad \text{.....................................} (53)$$

Putting the value of T(r) and T'(r) from equations (47) & (46) into equation (42), we get

$$U_r'' + (m_1+2)\frac{U_r'}{r} + 2\left(\frac{\mu m_1}{1-\mu}+1\right)\frac{U_r}{r^2} = \frac{1+\mu}{1-\mu}\alpha_0\left[(m_1+m_2)r^{m_2+1} \times \frac{-A_1}{(m_3+1)}r^{-(m_3+1)} + A_2 + r^{m_2+1} \times \left(\frac{-A_1}{r(m_3+1)}\right)\right]$$

Simplifying the right-hand side of the equation:

$$U_r'' + (m_1+2)\frac{U_r'}{r} + 2\left(\frac{\mu m_1}{1-\mu}+1\right)\frac{U_r}{r^2} = 1 - \mu\alpha_0\frac{A_1}{(m_3+1)}r^{m_2-m_3} - \mu\alpha_0\frac{A_2}{(m_3+1)}r^{m_2+1} - \mu\alpha_0\frac{A_1}{(m_3+1)}r^{m_2+1}$$

Let, $A_3 = -\mu\alpha_0\frac{A_1}{(m_3+1)}$ and $A_4 = -\mu\alpha_0\frac{A_2}{(m_3+1)}$, we get

$$U_r'' + (m_1+2)\frac{U_r'}{r} + 2\left(\frac{\mu m_1}{1-\mu}+1\right)\frac{U_r}{r^2} = A_3 r^{m_2+1} + A_4 r^{m_2-m_3} \quad \text{................................} (54)$$

Where,

$$A_3 = \frac{(1+\mu)(m_1+m_2)\alpha_0 A_2}{(1-\mu)} \quad \text{..} (55)$$

$$A_4 = \frac{(1+\mu)\left(1-\frac{m_1+m_2}{m_3+1}\right)\alpha_0 A_1}{(1-\mu)K_0} \quad \text{..} (56)$$

Equation (54) is the Euler differential equation.

The general solution is assumed to have the form.

$U_r^g(r) = Br^\eta$

Or$U_r' = \eta B r^{\eta-1}$ .... (57)

Or$U_r' = \eta(\eta-1)Br^{\eta-2}$

Substituting these expressions into equation (54), we get

$$\eta(\eta-1)Br^{\eta-2} + (m_1+2)\frac{\eta B r^{(\eta-2)}}{r} + 2\left(\frac{\mu m_1}{1-\mu}+1\right)\frac{Br^{(\eta-2)}}{r^2} = 1 + A_3 r^{(m_2+1)} + A_4 r^{(m_2-m_3)}$$

Multiplying both sides by r^2 and simplifying, we get:

$$\eta(\eta-1)Br^{\eta-2}+(m_1+2)\frac{\eta Br^{(\eta-2)}}{r}+2\left(\frac{\mu m_1}{1-\mu}+1\right)B=r^2+A_3r^{(m_2+3)}+A_4r^{(m_2-m_3+2)}$$

Rearranging and factoring out $Br^{(\eta-2)}$, we get

$$Br^{(\eta-2)}\left[\eta(\eta-1)r^2+(m_1+2)\eta r+2\left(\frac{\mu m_1}{1-\mu}+1\right)\right]=r^2+A_3r^{(m_2+3)}+A_4r^{(m_2-m_3+2)}$$

Since B and r are both non-zero, we can divide both sides by $Br^{(\eta-2)}$, we obtain:

$$\eta(\eta-1)r^2+(m_1+2)\eta r+2\left(\frac{\mu m_1}{1-\mu}+1\right)=\frac{r^2}{B\eta-2}+A_3r^{(m_2+3-\eta)}+A_4r^{(m_2-m_3+2-\eta)}$$

Now,

If we compare the above equation with equation, we see that the coefficients of the r^2 and r terms on both sides are equal, while the constant terms on both sides are equal, this means that the expression in the brackets on the left-hand side must be equal to 0.

$$\eta^{2+}(m_1+1)\eta+\left(\frac{\mu m_1}{1-\mu}+1\right)=0 \quad \text{……..……/……...……} \quad (58)$$

Equation (58) has two real roots η_1 and η_2

$$\eta_{1,2}=\frac{m_1+1}{2}\pm\left[\frac{(m_1+1)^2}{4}-2\left(\frac{\mu m_1}{1-\mu}+1\right)\right]\text{^0.5} \quad \text{…….……..……} \quad (59)$$

Thus, the general solution is

$$U_r^g(r)=B_1r^{\eta_1}+B_2r^{\eta_2}$$

The particular solution $U^P(r)$ is assumed to be of the form

$$U^P(r)=D_1r^{m_2+3}+D_2r^{m_2-m_3+2}$$

Taking first and second $U^P(r)$ is assumed to be of the form.

$$U^P(r)'=D_1(m_2+3)r^{(m_2+2)}+D_2(m_2-m_3+2)r^{(m_2-m_3+1)}$$

$$U^P(r)''=D_1(m_2+3)(m_2+2)r^{(m_2+1)}+D_2(m_2-m_3+2)(m_2-m_3+1)r^{(m_2-m_3)}$$

Substituting $U^P(r)$ and its derivatives in equation (54), we get

$D_1(m_2+3)(m_2+2)r^{(m_2+1)} + D_2(m_2-m_3+2)(m_2-m_3+1)r^{(m_2-m_3)+(m_1+2)}$

$= \frac{D_1(m_2+3)r^{(m_2+1)}+D_2(m_2-m_3+2)r^{(m_2-m_3+1)}}{r} \times \frac{2\left(\frac{\mu m_1}{1-\mu}+1\right)D_1 r^{(m_2+1)}}{r^2} + \frac{D_2 r^{(m_2-m_3+1)}}{r^2} = A_3 r^{(m_2+1)} + A_4 r^{(m_2-m_3)}$

Multiplying both sides by $r^{(m_3-m_2-2)}$ to simplify the coefficients of the terms on both sides, we get:

$D_1(m_2+3)(m_2+2)r^{(m_3-1)} + D_2(m_2-m_3+2)(m_2-m_3+1)r^{(m_3-1)} + (m_1+2)$
$D_1(m_2+3)r^{(m_3-m_1-1)} + D_2(m_2-m_3+2)r^{(m_3-m_1-1)}$

$2\left(\frac{\mu m}{1-\mu}+1\right)\left(D_1 r^{(m_3-m_2-1)}\right)+\left(D_1 r^{(m_3-m_2-m_3+2)}\right)=A_3 r + A_4$

This can be simplified further by grouping the terms with the same exponent of r, we get

$D_1\left[(m_2+3)(m_2+2)+(m_1+2)(m_2+3)+\left(\frac{\mu m_1}{1-\mu}-1\right)\right]r^{(m_3-m_2-1)} +$

$D_2\left[(m_2-m_3+2)(m_2-m_3+1)+(m_1+2)(m_2-m_3+2)+\left(\frac{\mu m_1}{1-\mu}-1\right)\right] r^{(m_3-m_2-m_3+2)} = A_3 r^{(1-m_2)} + A_4 r^{(m_3-m_2-m_3+2)}$

Simplifying,

$D_1\left[(m_2+3)(m_2+2)+(m_1+2)(m_2+3)+\frac{\mu m_1}{1-\mu}-1\right]r^{m_2+1} +$

$D_2\left[(m_2-m_3+2)(m_2-m_3+1)+(m_1+2)(m_2-m_3+2)+\frac{\mu m_1}{1-\mu}-1\right]r^{m_2-m_3+2}$
$=A_3 r^{m_2-1} + A_4 r^{m_2-m_3}$ …………………………………………………..……….. (60)

Now, equating the coefficient of identical powers yields.

$D_1 = \frac{A_3}{\left[(m_2+3)(m_2+2)+(m_1+2)(m_2+3)+\left(\frac{\mu m_1}{1-\mu}-1\right)\right]}$

$D_2 = \frac{A_4}{(m_2-m_3+2)(m_2-m_3+1)+(m_1+2)(m_2-m_3+2)+\frac{\mu m_1}{1-\mu}-1}$ ……………..……..…………………..….... (61)

The complete solution for U(r) is the sum of the general & particular solutions as

U(r) $= U^g(r) + U^P(r)$

Thus,

U(r) = $B_1 r^{\eta 1} + B_2 r^{\eta 2} + D_1 r^{m_2+3} + D_2 r^{m_2-m_3+2}$ ……..…..…… (62)

Substituting equations (62) into equations (33), (34) & (35) yields,

Starting with equation (33),

$\varepsilon_r = \frac{dU_r}{d_r}$; $\varepsilon_\emptyset = \varepsilon_\theta = \frac{u_r}{r}$

We substitute the expression for $U(r)$ from equation (62) into $\varepsilon_\emptyset = \varepsilon_\theta$ and simplify:

$\frac{U_r}{r} = \frac{\left(B_1 r^{\eta 1} + B_2 r^{\eta 2} + D_1 r^{m_2+3} + D_2 r^{m_2-m_3+2}\right)}{r}$

$= B_1 r^{\eta 1-1} + B_2 r^{\eta 2-1} + D_1(m_2+3) r^{(m_2+2)} + D_2(m_2 - m_3 + 2) r^{(m_2-m_3+1)}$

Therefore, the strain components become:

$\varepsilon_r = \frac{dU_r}{d_r} = \eta_1 B_1 r^{\eta 1-1} + B_2 r^{\eta 2-1} + D_1(m_2+3) r^{(m_2+2)} + D_2(m_2 - m_3 + 2) r^{(m_2-m_3+1)}$

$\varepsilon_\emptyset = \varepsilon_\theta = \frac{U_r}{r} = B_1 r^{\eta 1} + B_2 r^{\eta 2} + D_1 r^{m_2+3} + D_2 r^{m_2-m_3+2}$ ……..... (63)

Next, we substitute the expression for $U(r)$ from equation (62) into equation (34) & (35) and simplify:

Starting with equation (34)

$\sigma_r = \frac{E}{(1-2\mu)(1+\mu)} \left((1-\mu)\frac{dur}{dr} + 2\mu \frac{Ur}{r} - (1+\mu)\alpha T\right)$

Substituting for $\frac{dur}{dr}$ & $\frac{Ur}{r}$:

$\sigma_r = \frac{E}{(1-2\mu)(1+\mu)} \times$

$\left[(1-\mu)\eta_1 B_1 r^{\eta_1-1} + B_2 r^{\eta_2-1} + D_1(m_2+3) r^{(m_2+2)} + D_2(m_2 - m_3 + 2) r^{(m_2-m_3+1)} + \frac{2\mu\left(B_1 r^{\eta 1} + B_2 r^{\eta 2} + D_1 r^{(m_2+3)} + D_2 r^{(m_2-m_3+2)}\right)}{r} - (1+\mu)\alpha T\right]$

Simplifying,

$\sigma_r = \frac{E_o r^{m1}}{(1-2\mu)(1+\mu)} \{(1-\mu)\eta_1 + 2\mu\} B_1 r^{\eta_1-m_1-1} + \{(1-\mu)\eta_2 + 2\mu\} B_2 r^{\eta_1-m_1-1} +$

$\{(1-\mu)(m_2+3) + 2\mu\} D_1 r^{m_1-m_2-2} +$

$\{(1-\mu)(m_3 - m_2 + 2) + 2\mu\} D_1 r^{m_1-m_2-m_3-1} -$

$(1+\mu)\alpha_0 A_2 r^{m_1-m_2} + \frac{\alpha_0 A_1(1+\mu)}{K_0(m_3+1)} r^{m_1-m_2-m_3-1}$ …….…… (64)

Now, substituting equation (62) into equation (35), we get

$\sigma_\emptyset = \frac{E}{(1-2\mu)(1+\mu)} \left[\frac{Ur}{r} + \mu \frac{dur}{dr} - (1+\mu)\alpha T\right]$

Substituting the expression $\varepsilon_r$that we obtained earlier and the expression for U_r that was given earlier, we get

$\sigma_\emptyset = \frac{E_o}{(1-2\mu)(1+\mu)} (1+\mu\eta_1)B_1 r^{\eta_1-m_1-1} + (1+\mu\eta_2)B_2 r^{\eta_1-m_1-1} + \{1+\mu(m_2+3)\} D_1 r^{m_1-m_2-2} + \{1+\mu(m_2-m_3+2)\}D_2 r^{m_1-m_2-m_3-1} + (1+\mu)\alpha_0 A_2 r^{m_1-m_2} + \frac{\alpha_0(1+\mu)}{K_0(m_3+1)} r^{m_1-m_2-m_3-1}$ …… (65)

The boundary condition for stresses given by,

σ_r(a) = -p; σ_r(b) = $-p_0$ ……..…… (66)

Equation (64) represents the stress distribution within a spherical shell subjected to internal pressure. Equation (66) represents the boundary conditions for stresses at the inner & outer radii of the shell.

Substituting the boundary conditions (66) into equation (64), the constant of integration becomes;

at, r = a

$\sigma_r(a) = -p = \frac{-E_o a^{m1}}{(1-2\mu)(1+\mu)} \{(1-\mu)\eta_1 + 2\mu\} B_1 a^{\eta_1-m_1-1} + \{(1-\mu)\eta_2 + 2\mu\} B_2 a^{\eta_1-m_1-1} + \{(1-\mu)(m_2+3)+2\mu\} D_1 a^{m_1-m_2-2} + \{(1-\mu)(m_3-m_2+2)+2\mu\} D_1 a^{m_1-m_2-m_3-1} - (1+\mu)\alpha_0 A_2 a^{m_1-m_2} + \frac{\alpha_0 A_1(1+\mu)}{K_0(m_3+1)} a^{m_1-m_2-m_3-1}$

at, r = b

$\sigma_r(b) = -p_0 = \frac{E_o b^{m1}}{(1-2\mu)(1+\mu)} \{(1-\mu)\eta_1 + 2\mu\} B_1 b^{\eta_1-m_1-1} + \{(1-\mu)\eta_2 + 2\mu\} B_2 b^{\eta_1-m_1-1} + \{(1-\mu)(m_2+3)+2\mu\} D_1 b^{m_1-m_2-2} + \{(1-\mu)(m_3-m_2+2)+2\mu\} D_1 b^{m_1-m_2-m_3-1} - (1+\mu)\alpha_0 A_2 b^{m_1-m_2} + \frac{\alpha_0 A_1(1+\mu)}{K_0(m_3+1)} b^{m_1-m_2-m_3-1}$

Simplify,

$$-d_1B_1 - d_2B_2 - d_5 + \frac{(1+\mu)\alpha_0 A_1}{K_0 a^{m_3-m_2+1}} = p$$

$$-d_3B_1 - d_4B_2 - d_6 + \frac{(1+\mu)\alpha_0 A_2}{b^{m_3+1}} = p_0$$

We rearrange the equations to isolate the constant of integration:

$$B_1 = \frac{(d_4d_7+d_4d_5)-(d_2d_8+d_2d_6)}{(d_1d_4-d_2d_3)} \quad \text{..... (67)}$$

$$B_2 = \frac{(d_3d_7+d_3d_5)-(d_1d_8+d_1d_6)}{(d_2d_3-d_1d_4)} \quad \text{..... (68)}$$

The values of $d_1, d_2, d_3, d_4, d_5, d_6, d_7$ & d_8 are obtained by substituting the boundary conditions (66) in equation (64).

Starting with d_1, we can write the stress σ_r(a) as;

$$\sigma_r(\text{a}) = -\text{p} = \frac{-E_o a^{m1}}{(1-2\mu)(1+\mu)}\{(1-\mu)\eta_1 + 2\mu\}B_1 a^{\eta_1-m_1-1} + \{(1-\mu)\eta_2 + 2\mu\}B_2 a^{\eta_1-m_1-1} + \{(1-\mu)(m_2+3)+2\mu\}D_1 a^{m_1-m_2-2} + \{(1-\mu)(m_3-m_2+2)+2\mu\}D_1 a^{m_1-m_2-m_3-1} - (1+\mu)\alpha_0 A_2 a^{m_1-m_2} + \frac{\alpha_0 A_1(1+\mu)}{K_0(m_3+1)} a^{m_1-m_2-m_3-1}$$

Since we know the value of p, we can substitute it in the above equation and simplify it to obtain d_1:

$$d_1 = \{(1-\mu)\eta_1 + 2\mu\}a^{\eta_1+m_1-1}$$

Similarly, we can substitute the value of σ_r(b) = $-p_0$ in equation (64) to get the expression for d_3,

$$d_3 = \{(1-\mu)\eta_1 + 2\mu\}b^{\eta_1+m_1-1}$$

To obtain d_2 & d_4, we need to use the values of σ_r(a) & σ_r(b) in the expression for B_1 & B_2 in (67) & (68), respectively. Substituting the values of equations (67) & (68) and simplifying, we get;

$$d_2 = \{(1-\mu)\eta_2 + 2\mu\}a^{\eta_2+m_1-1}$$

$d_4 = \{(1-\mu)\eta_2 + 2\mu\}b^{\eta_2+m_1-1}$

For d_5 & d_6, we substitute the value of σ_r(a) & σ_r(b) in the expression for $\alpha_0 A_2 a^{m_1-m_2}$ and $\alpha_0 A_2 b^{m_1-m_2}$, respectively in equation (64), we get

$d_5 = (1+\mu)\alpha_0 a^{m_1+m_2} A_2$

$d_6 = (1+\mu)\alpha_0 b^{m_1+m_2} A_2$

Finally, for d_7 & d_8 we substitute the values of σ_r(a) & σ_r(b) in the expression for $D_1 a^{m_1-m_2-2}, D_1 b^{m_1-m_2-2}, D_2 a^{m_1-m_2-m_3-1}$ and $D_2 b^{m_1-m_2-m_3-1}$ and simplify to obtain;

$d_7 = -(1+\mu)(1-2\mu)\frac{P_O}{E_O} - \{(1-\mu)(m_2+3)+2\mu\}D_1 a^{m_1+m_2+2} - \left[\{(1-\mu)(m_2 - m_3+2)+2\mu\}D_2 + \frac{(1+\mu)\alpha_0 A_1}{K_0(m_3+1)}\right] a^{m_1+m_2-m_3-1}$

$d_8 = -(1+\mu)(1-2\mu)\frac{P_O}{E_O} - \{(1-\mu)(m_2+3)+2\mu\}D_1 b^{m_1+m_2+2} - \left[\{(1-\mu)(m_2 - m_3+2)+2\mu\}D_2 + \frac{(1+\mu)\alpha_0 A_1}{K_0(m_3+1)}\right] b^{m_1+m_2-m_3-1}$ …….. (69)

2.4 VALIDATION OF THEORETICAL MODEL

In order to authenticate the present investigation, a validation of the theoretical model has been carried out in terms of the non-dimensional pressure variation with respect to various thickness of the spherical shell, by comparing the present work with the work of S. Saha et al. (2011) and depicted in the figure 2 and 3 respectively. In both figures, the red colored curves show the non-dimensional pressure variation with respect to the thickness of the spherical shell with considering autofrettage technology, and the blue colored curves depict the same variation without considering autofrettage technology. From both the above mentioned figures 2 and 3, it is noted that the pressure withstand capacity of an autofrettage treated spherical shell increases with increasing thickness of the shell. On the other hand, the pressure withstand capacity of non-autofrettage shell initially increased with increasing shell thickness, but after a certain limit of thickness, it is fixed and becomes constant.

In the present work, a curve has been plotted with respect to thickness of the spherical shell considering $\frac{P}{\sigma_y}$ of 0.6. S. Saha et al (2011) has been presented the same variation for the $\frac{P}{\sigma_y}$ of 0.5. The nature of both curves shows good agreement between the present theoretical work and the work presented by S. Saha et al (2011). A slight variation has been observed due to the variation in considering the value of $\frac{P}{\sigma_y}$.

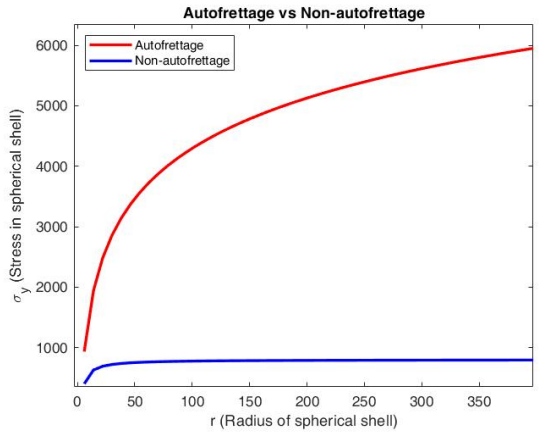

Figure 2. Autofrettage Vs Non-Autofrettage for $\frac{P}{\sigma_y}$ of 0.6 (present work)

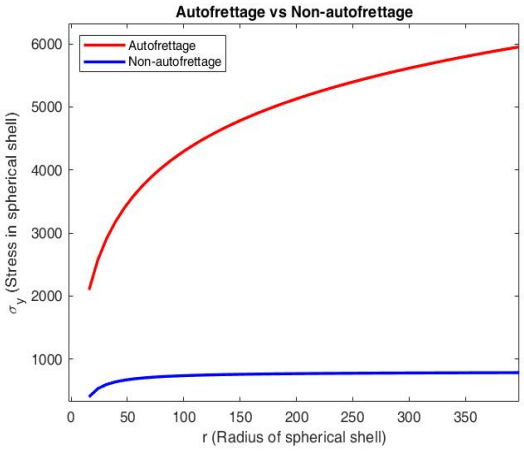

Figure 3. Autofrettage Vs Non-Autofrettage for $\frac{P}{\sigma_y}$ of 0.5 depicted by S. Saha et al. (2011)

CHAPTER 3

3. RESULTS & DISCUSSION:

The result of the present study is presented in this section.

3.1 Determination of the optimum radius of the elastic-plastic junction, c_{opt}:

Figure 4 shows the relationship between the pressure (P) applied and the radius of the elastic-plastic junction (c_{opt}). By analyzing equation (20), it becomes evident that the influence of the applied pressure and yield strength on c_{opt} can be directly depicted. When the applied pressure (P) is high, indicating a thicker wall for the spherical shell, the value of c_{opt} should also be higher. This is because a higher c_{opt} allows the shell to have an increased load-bearing capacity. Therefore, equation (20) provides a means to determine c_{opt} accurately, considering the influence of both the applied pressure and the material's yield strength. Figure 4 shows that as the pressure inside the spherical shell is increased, the optimal elastic-plastic radius juncture is increased, and also the strength of the material is increased.

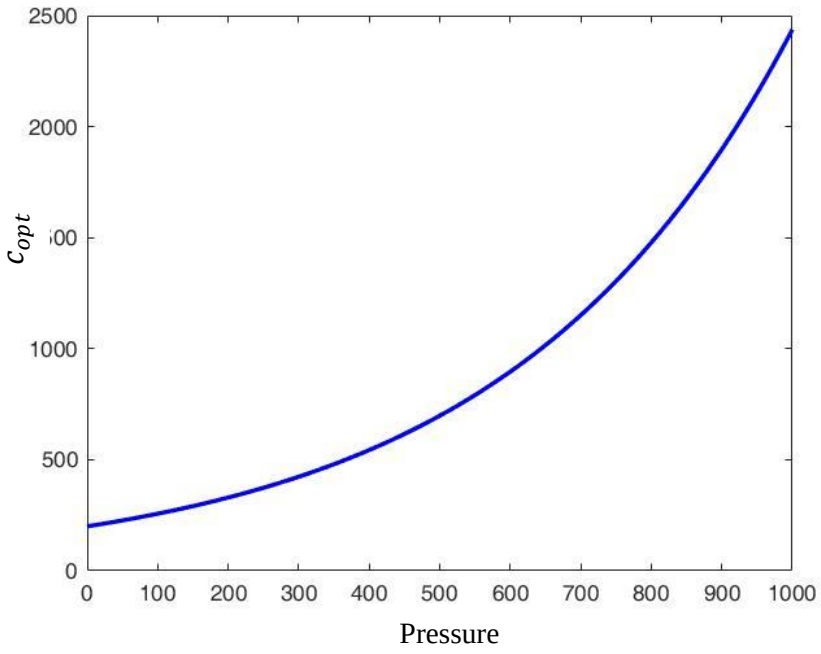

Figure 4. Relation between c_{opt} and P

3.2 Influence of autofrettage on a spherical shell:

Equation (21) represents the maximum allowable pressure p_a^{iv} for an autofrettaged spherical shell. It indicates the maximum pressure that an autofrettaged spherical shell can withstand while maintaining its elastic behavior. Equation (23) and equation (21) demonstrate that the

increase of the elastic strength of a non-autofrettage spherical shell is limited (the limit is p_e^{iv} = $\frac{2\sigma_y}{3}$), even if its thickness is increased infinitely, while an autofrettage spherical shell has limitless strength if the thickness is increased infinitely, as shown in figure 5.

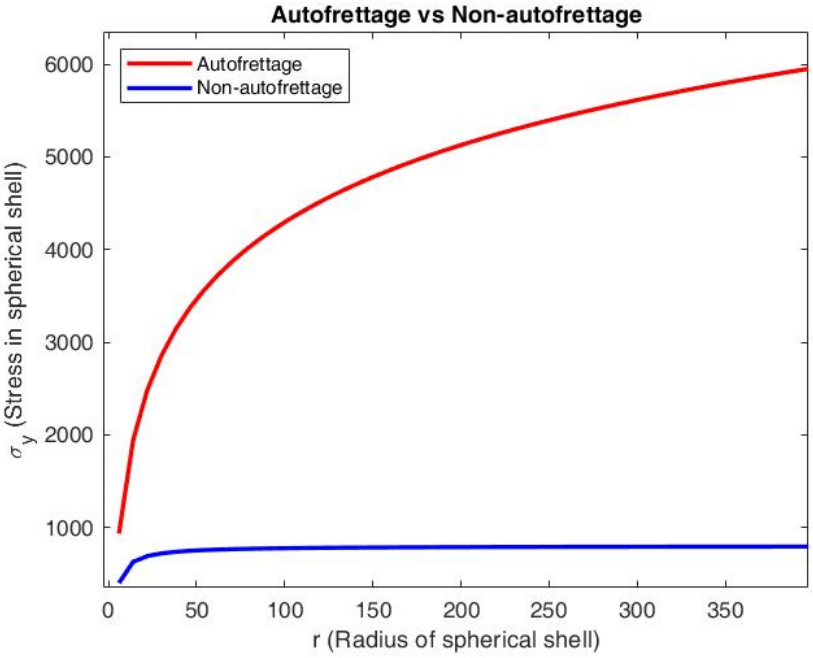

Figure 5. Autofrettage Vs Non-autofrettage

3.3 Determination of optimum autofrettage pressure of a thick spherical shell:

Autofrettage is a process in which a high internal pressure is applied to a shell before it is put into use, with the aim of inducing yielding on its inner surface and achieving a desired level of residual stresses c_{opt}. The Von Mises strength theory was employed to derive the equation for the autofrettage pressure. The equation (25) represents the autofrettage pressure p_a^{iv} according to the Von Mises strength theory. The relationship between p_{aopt} and p is seen in equation figure 6, from which we can determine that p_{aopt} must be larger than p; otherwise, the wall of a spherical shell does not yield.

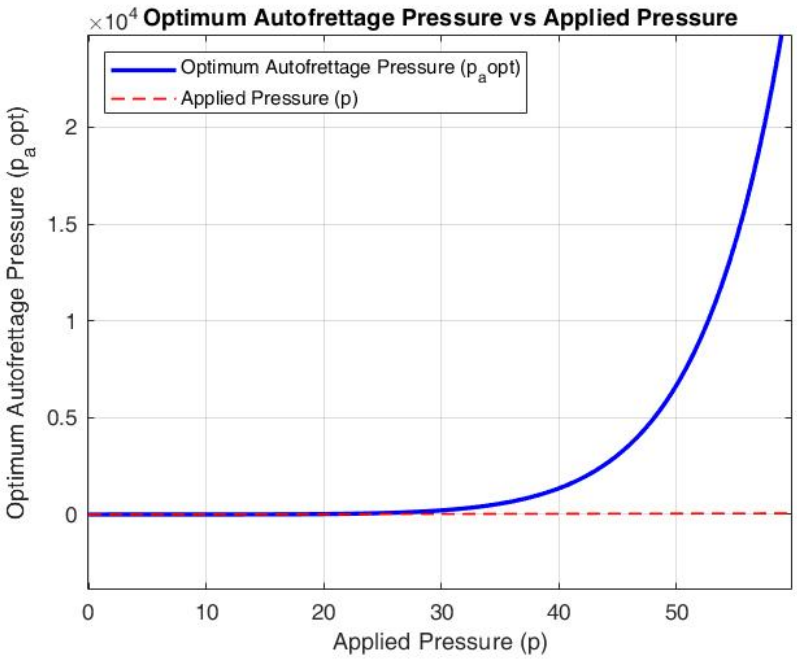

Figure 6. Relation between p_{aopt} and p

In this work, we have considered a functionally graded hollow thick spherical vessel of outer radius $b = 1.2$m and inner radius $a = 1$m; the thermal coefficient of expansion (K) and the modulus of elasticity (E) at the inner radius is α_t=1.2 x 10^{-6}/°c and E = 200GPa respectively and the Poisson ratio (μ) to be 0.3. For simplicity of analysis, the power law co-efficient for K, E, and α is considered to be the same, i.e., $m_1 = m_2 = m_3 = m$. The boundary condition for temperature is taken as T(b) = 0 and T(a) =10°C.

Figure 7 shows the temperature fluctuation in the radial direction for various power law index (m) values obtained from Equation (47). The Figure 7 demonstrates that for m > 1, as the power law index m increases, so does the temperature. This indicates that a higher power law index leads to higher temperature distributions within the spherical shell. From the Table 1, the temperature distribution at a radial distance of 1.1 for different power law index (m) within the functionally graded spherical shell is presented. For a radial distance of 1.1, the temperature values are recorded for three different power law indexes: 2.1, 2.2, and 2.5. For a power law index of 2.1, the recorded temperature at a radial distance of 1.1 is 3.27°C. With a slightly higher power law index of 2.2, the temperature increases to 3.29°C. Lastly, for a power law index of 2.5, the temperature reaches its highest value at 3.33°C. These observations are consistent with the theory that a higher power law index corresponds to higher temperature distributions within the spherical shell. As the power law index increases from 2.1 to 2.5, the temperature progressively rises, indicating a direct relationship between the power law index

and temperature. This behaviour can be explained, as m increases, the material becomes stiffer, which results in reduced heat dissipation and, consequently, higher temperatures.

Table 1. Variation of Temperature for different power law of index

Radius (m)	Power law index (m)	Temp °c
1.1	2.1	3.27
1.1	2.2	3.29
1.1	2.5	3.33

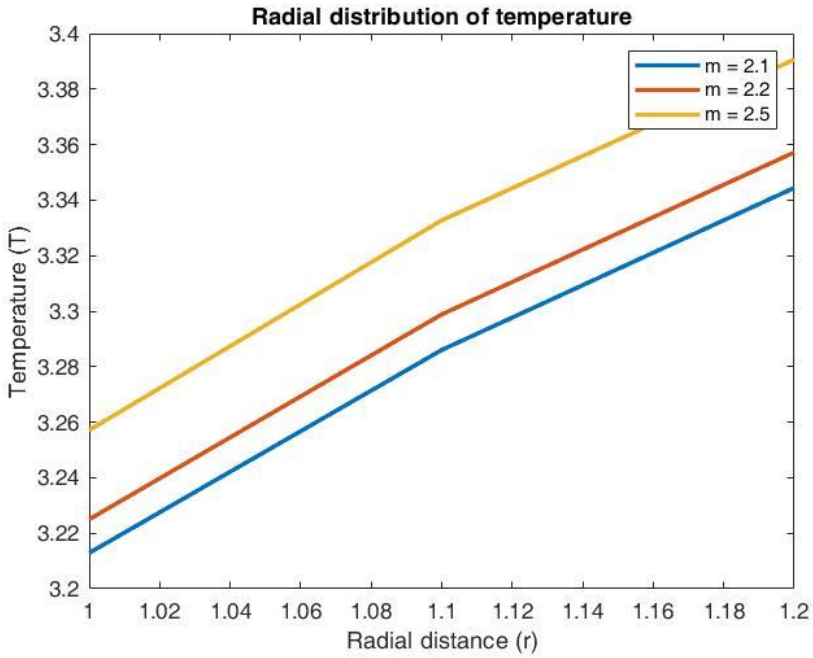

Figure 7. Radial Distribution of Temperature for different power law of index

Figure 8 depicts the variation in the distribution of radial stress along the radial direction as calculated from equation (64). The Figure has shown that for, m < 1, as the power law index decreases, the radial stress increases. This implies that a decrease in the power law index leads to an increase in the magnitude of the radial stress. From the Table 2, a power law index of 0.9, the radial stress at a radial distance of 1.1 is recorded as 2.72. With a lower power law index of 0.7, the radial stress increases to 2.77. Further, reducing the power aw index to 0.5 results in an increase in the radial stress to 2.83. This demonstrates that an increase in the magnitude of the radial stress follows a decrease in the power law index. A smaller power law index (m < 1) in the case of radial stress distribution denotes that material characteristics, such as the elasticity

modulus (E), decrease rapidly from the inner to the outer radius. The material in this case is stiffer at the inner radius than it is towards the outside radius. The stiffer inner portion helps to distribute the external load more evenly across the entire component, reducing the stress concentration at the inner surface. This leads to more uniform stress distribution and minimizes the risk of failure or damage.

Table 2. Variation of Radial stress for different power law of index

Radius (m)	Power law index (m)	Radial stress
1.1	0.9	2.72
1.1	0.7	2.77
1.1	0.5	2.83

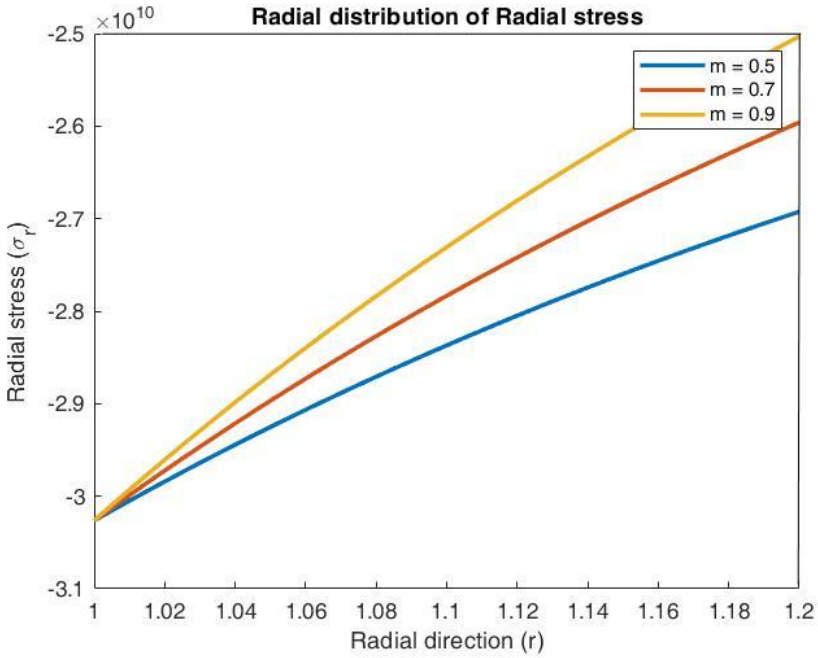

Figure 8. Radial Distribution of Radial Stress for different power law of index

Figure 9 shows the hoop stress variation along the radius, derived from equation (65). From the Table 3, power law index of 0.8, the recorded circumferential stress at a radial distance of 1.1 is 9.24. With a slightly lower power law index of 0.7, the circumferential stress increases to 9.34. Further, a circumferential stress increase of 9.38 is produced by reducing the power law index to 0.5. We observe that for, $m < 1$, a drop in the power law index results in an increase in the hoop stress, which is similar to the radial stress. Figure 9 also shows that, independent

of the power law index number, the hoop stress decreases as you increase the radius. In other words, for a given power law index value, hoop stress is higher towards the inner radius of the component and gradually decreases as we move toward the outer radius.

Table 3. Variation of Circumferential stress for different power law of index

Radius (m)	Power law index (m)	circumferential stress
1.1	0.8	9.24
1.1	0.7	9.34
1.1	0.5	9.38

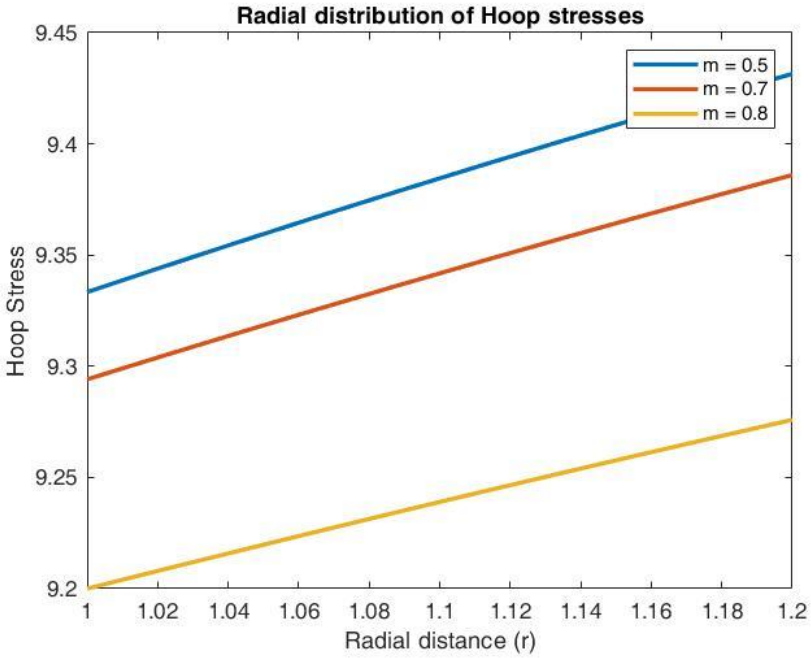

Figure 9. Radial Distribution of Hoop Stress for different power law of index

CHAPTER 4

CONCLUSION

In conclusion, this theoretical study focused on analyzing the impact of internal pressure on a functionally graded hollow spherical shell. The material properties were assumed to exhibit a non-linear behavior with a power law distribution along the graded direction. The Navier and heat conduction equations were solved using a direct method to investigate the influence of internal pressure and temperature on the design of pressure vessels.

The findings of this research include the presentation of pressure variation, mechanical stress distribution (radial stress and hoop stress), and radial temperature distribution in a sequential manner. Based on the obtained results, it can be concluded that materials with lower power law index are advantageous in terms of minimizing thermal stress generation. The results demonstrate that autofrettage increases the internal pressure within the shell, thereby improving its ability to withstand higher internal pressures. The Following conclusions has been drawn from this thesis work.

1. The variation of temperature along the radial direction is influenced by the power law index, with higher values of the index resulting in higher temperatures.
2. The theoretical study focuses on the effect of internal pressure in a functionally graded hollow spherical shell, considering non-linear material properties with a power law distribution.
3. To examine how internal stresses and temperature affect the pressure vessel's design, the Navier and heat conduction equations are solved.
4. The thesis presents the pressure variation, as well as the distribution of mechanical stresses such as radial stress and hoop stress along the radial direction.
5. A higher power law index results in increased temperature.
6. Autofrettage significantly reduces tension in the inner part of the spherical shell.
7. It has been observed that an autofrettage treated spherical shell has limitless strength if the thickness is increased infinitely.
8. Yielding will not occur in the wall of the spherical shell if p_{aopt} is not a little bit larger than p.

NOMENCLATURE

ε_r = Radial strain

$\varepsilon_\emptyset$ = Circumferential strain

σ_r = Radial stress

$\sigma_\emptyset$ = Circumferential stress

E = Modulus of Elasticity

μ = Poisson's ratio

α = coefficient of thermal expansion

T = Temperature

α_T = Thermal coefficient of expansion

m = power law of index

K = Thermal conductivity

r = Radial distance

λ & G = Lame's coefficient

U_g = General solution

U_p = particular solution

C_{opt} = Optimum radius of elastic-plastic juncture

σ_y = Yield stress

P' = Initial pressure

P_{aopt} = Optimum autofrettage pressure

REFERENCES

1) Anthony P. Parker., (2001) **Autofrettage of Open-End Tubes-Pressures, Stresses, Strains, and Code Comparisons**, Journal of Pressure Vessel Technology, Vol. 123, pp 271-281.

2) M. Jabbari, S. Sohrabpour, M.R. Eslami., (2002) **Mechanical and Thermal stresses in a functionally graded hollow cylinder due to radially symmetric loads**, International journal of Pressure Vessels and Piping, 79, pp 493-497.

3) Jesus Manuel Alegre Calderon, P.M. Bravo, Monica Preciado., (2005) **Design of an autofrettaged high-pressure vessel, considering the Bauschinger effect**, Proc. IMechE Vol. 220 Part E: J. Process Mechanical Engineering.

4) R. Shahsiah, M.R. Eslami and R. Naj., (2006) **Thermal Instability of functionally Graded Shallow Spherical Shell**, Journal of Thermal Stresses, 29:8, 771-790.

5) Rahman Seifi, Majid Babalhavaeji., (2011) **Bursting pressure of autofrettaged cylinders with inclined external cracks**, International Journal of Pressure Vessels and Piping. 112-119.

6) Prabir Chandra Bhattacharyya, Sujoy Saha, Samar C. Mondal., (2011) **Autofrettage of a Thick Spherical Shell**, J.Mech.ont. & Math.sci., Vol-5, No.-2, pp 643-654.

7) Zhong Hu, Sudhir Puttagunta., (2012) **Computer Modelling of internal pressure Autofrettage Process of a Thick-Walled Cylinder with the Bauschinger Effect**, American Transactions on Engineering & Applied Sciences, Volume 1 No.2,

8) Niranjan Kumar., (2012) **Optimization of Autofrettage-Reautofrettage Percent and Shrink-Fit Combination for Optimum Fatigue Life in Multilayer Pressure Vessels**, Journal of Applied Mechanical Engineering, Vol. 1, Issue 3.

9) Dr. Pankaj Thakur., (2012) **Analysis of Stresses in a Spherical Shell Subjected to Internal Pressure**, IJMEC; Vol. 3, No. 2, pp 89-96.

10) M. Sedighi, A.H. Jabbari., (2013) **Investigation of residual stresses in thick-walled vessels with a combination of autofrettage and wire-winding,** International Journal of Pressure Vessels and Piping.

11) Tanjin Amin, Dr. Abu Rayhan Md. Ali, Tousif Ahmed and Faisal Ahmed., (2013) **Optimum Design of Autofrettaged Thick-Walled Cylinders**, Global Journal of Researches in Engineering Mechanical and Mechanics Engineering, Volume 13 Issue 8 Version 1.0.

12) D. Dinesh Babu, T. Jegan Balaji., (2013) **Theoretical and Finite Element Analysis of High-Pressure Components**, IOSR Journal of Engineering, Vol. 3, Issue 2.

13) Gennadiy Lvov, Olga Kostromitskaya., (2014) **Effect of Material Damage on Autofrettage of Thick-Walled Cylinder**, Universal Journal of Mechanical Engineering 2(2):44-48.

14) S.P. Pawar, K.C. Deshmukh, G. D. Kedar., (2015) **Thermal stresses in functionally graded hollow sphere due to non-uniform internal heat generation**, International Journal of Application and Applied Mathematics, Vol 10, Issue 1, pp. 552-569.

15) Rupali, S.C. Mondal, S. Sarkar., (2017) **Analytical and Finite Element Analysis of Thermal Autofrettage process in Spherical vessel**, Journal of Mechanical and Civil Engineering (IOSR-JMCE), Vol 14, Issue 3 Ver. II.

16) Ruilin Zhu, Guolin Zhu, Aifeng Mao., (2017) **Mechanical Analysis of Autofrettaged High-Pressure Apparatus**, Journal of Theoretical and Applied Mechanics, 55, 1, pp. 17-27, Warsaw.

17) Marina Rynkovskaya, Sergei Alexandrov and Lihui Lang., (2019) **A theory of Autofrettage for Open-Ended, Polar Orthotropic Cylinders**, Symmetry.

18) Ritu.J. Singh, Ramesh Kumar, J. Mishra, V. Balasubram5anian., (2019) **Study the Effect of Anisotropy of Elastic-Plastic properties on Residual Stress Development in Autofrettage of Thick Cylinder**, Procedia Structural Integrity, 14, pp 549-555.

19) Guiqin Li., (2021) "**Research on Autofrettage Mechanism in Ultra-High Pressure Thick-walled Vessel, Journal** of Physics.

20) Mengjun ZHAO, Pengchen ZHU, Zan LIU, Chao KANG., (2021) **Mechanical Analysis for Two-layered Ultrahigh Pressure Apparatus with Interlayer Pressure**, Mechanical Engineering Science, Vol. 3, No. 1